Graduate Theses and Dissertations                                    Graduate School

2011

# Novel Film Formation Pathways for Cu2ZnSnSe4 for Solar Cell Applications

Sree Satya Kanth Bendapudi
*University of South Florida*, sbendapu@mail.usf.edu

Follow this and additional works at: http://scholarcommons.usf.edu/etd

Part of the American Studies Commons, and the Electrical and Computer Engineering Commons

Novel Film Formation Pathways for $Cu_2ZnSnSe_4$ for Solar Cell Applications

by

Sree Satya Kanth Bendapudi

A thesis submitted in partial fulfillment
of the requirements for the degree of
Master of Science in Electrical Engineering
Department of Electrical Engineering
College of Engineering
University of South Florida

Major Professor: Don L. Morel, Ph.D.
Christos Ferekides, Ph.D.
Andrew Hoff, Ph.D.

Date of Approval:
March 14, 2011

Keywords: Kesterite, Bandgap, Diffusion, XRD, Characterization

# DEDICATION

I want to dedicate my thesis to my parents and family for all their years of love and support. My father in particular has been my best teacher ever.

Thank you GOD.

## ACKNOWLEDGEMENTS

This thesis would not have been possible without the guidance and the help of several individuals who in one way or another contributed and extended their valuable assistance in the preparation and completion of this study.

First and foremost, my utmost gratitude to my supervisor, Dr. Don Morel, his inspiration, guidance and support has guided me all throughout my masters. I am very thankful to him for giving me this golden opportunity to work under him.

Dr. Chris Ferekides who has always been there to correct me and convert my mistakes into stepping-stones.

A special thanks to Sheetal kumar Chanda who introduced me to this field of research and guided me through the initial stages of my masters. Vassilis Palekis and Deidra Hodges for their immense support, sharing their experiences and knowledge during the time of study. Ryan Anders for patiently testing all my samples and correcting things. Keshavanand Jayadevan who stood beside me in every situation to extend his helping hand. Lab mates Kartikay Singh and Yejiao Wang without whom the lab goes dead and boring. A special thanks to my best friend Venkatesh Katari who always believed in me, supported me and encouraged me to give it the best in whatever I do.

**TABLE OF CONTENTS**

# LIST OF TABLES

# LIST OF FIGURES

**ABSTRACT**

Because of the anticipated high demand for Indium, ongoing growth of CIGS technology may be limited. Kesterite materials, which replace In with a Zn/Sn couple, are thought to be a solution to this issue. However, efficiencies are still below the 10% level, and these materials are proving to be complex. Even determination of the bandgap is not settled because of the occurrence of secondary phases. We use a film growth process, 2SSS, which we believe helps control the formation of secondary phases. Under the right growth conditions we find 1/1 Zn/Sn ratios and XRD signatures for $Cu_2ZnSnSe_4$ with no evidence of secondary phases. The optical absorption profile of our films is also a good match to the CIS profile even for films annealed at 500° C. We see no evidence of phase separation. The effect of intentional variation of the Zn/Sn ratio on material and device properties is also presented.

# 1. INTRODUCTION

This document gives a detailed analysis for the synthesis of thin film growth of the compound $Cu_2ZnSnSe_4$ also known as CZTSe by novel reaction pathways. The method involves glass substrates on which the metals are deposited in different orders and is then heated at a certain substrate temperature in the presence of selenium flux. There is a lot of research going on right now around the word on various ways of thin film production. In chapter 2 we would go through the literature review of these various thin film techniques and more focus would be given to CZTSe films. From now on CZTSe would be called CZSS throughout this document. Also we would be discussing why Tin and Zinc are replacing Indium in CIS based absorber layers to be called the CZSS absorber layer. Chapter 3 talks about our approach to making CZSS and discusses in detail why we think it is advantageous over other techniques. We would discuss in detail the diffusion phenomenon at the various stages of selenization, the metal selenide precursors, which we encounter, is a complex composite of both kinetics and thermodynamics. Chapter 4 consists of the results of various optical and characterization measurements on the samples. Retaining the metal content and maintaining the composition of the sample was a complex task. The variation in the substrate temperature and method implemented in selenization were critical factors in attaining the stoichiometry of the absorber material. Device parameters like bandgap were studied

through optical measurements like transmission test. The structures of the samples were determined by X-ray Diffraction spectroscopy. The statistics obtained in XRD proved interesting facts regarding the actual Kesterite compound and the precursor material ZnSe. From the analysis and results obtained on CZSS growth techniques and device performance I recommend in applying this recipe to large-scale manufacturing.

Before we go into details of things I would want to present some background information on the conventional and alternative energy sources and demand in the present day world, energy conversion from photovoltaic's, some introduction on thin films and all the available technologies by which they are synthesized. And finally we would go through some literature review on Kesterite-based thin film solar cells.

# 2. BACKGROUND

## 2.1 Review of Traditional Electricity Generation Technology

For millennia man has always been on the hunt for ways by which he could produce energy. The evolution and advancement in energy production goes back to days when nomadic man invented fire from rubbing two stones to the present world where every function done involves various sources of energy like fossil fuels, natural gas, hydro, nuclear, geothermal, solar, etc. Cost wasn't a criterion in the primitive world when resources were in abundance. As man evolved so did his needs for energy consumption. With a present world population of more than 6.5 billion and an estimated figure of 10 billion by 2055[1], there is a serious task on hand to look for energy sources, which explored wont alter the ecological balance. These sources as we know are called the renewable sources of energy.
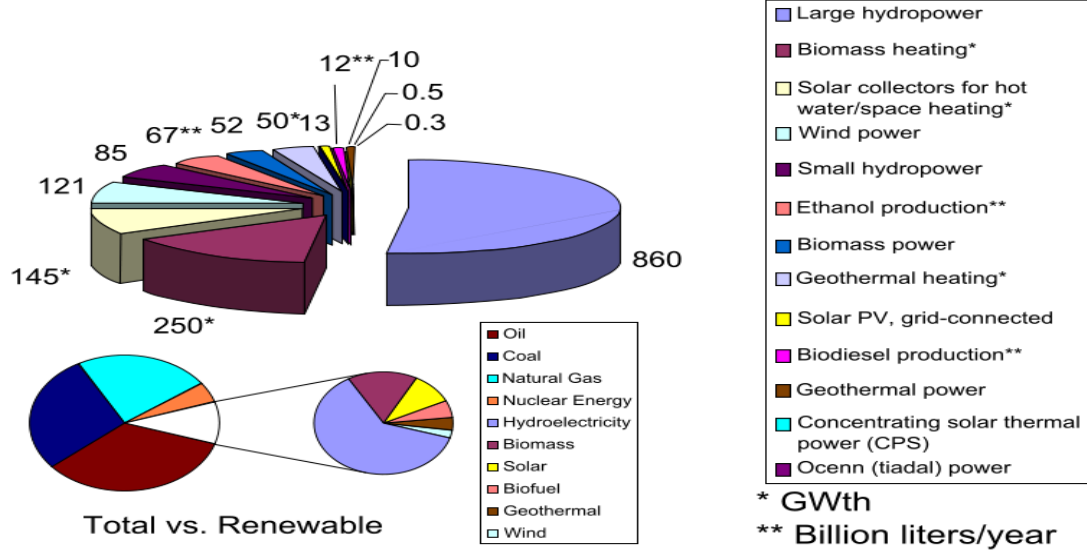
Fig. 2.1. Comparison of the various renewable energy production sources with each other and with the total energy production. [2]

Over dependence on non-renewable sources by man till date has pushed them to the limit of scarcity and couple of decades down the lane, extinction. We have also witnessed the disadvantages in it like pollution, irreversible damage to the environment, escalation of price of the fuel day by day and most importantly they eventually run out. These situations can only be avoided if we are able to make the transition to renewable sources and that too, as soon as possible. But the two major limitations faced in synthesizing energy from renewable sources are the cost and efficiency. The cost to generate electricity from coal is around $0.04/KW/h and from gas and oil is a little bit more but around $0.08/KW/h. Given below is a plot which shows the current prices on electricity production by various renewable energy sources. The wind, geothermal and hydro electricity are priced around the range $0.05-0.07/KW/h but solar (PV) still

4

remains expensive at around $0.19/KW/h. With extensive research gong into each of these energy sources the prices are estimated to drop in the next couple of years. This is shown in Fig. 2.3.
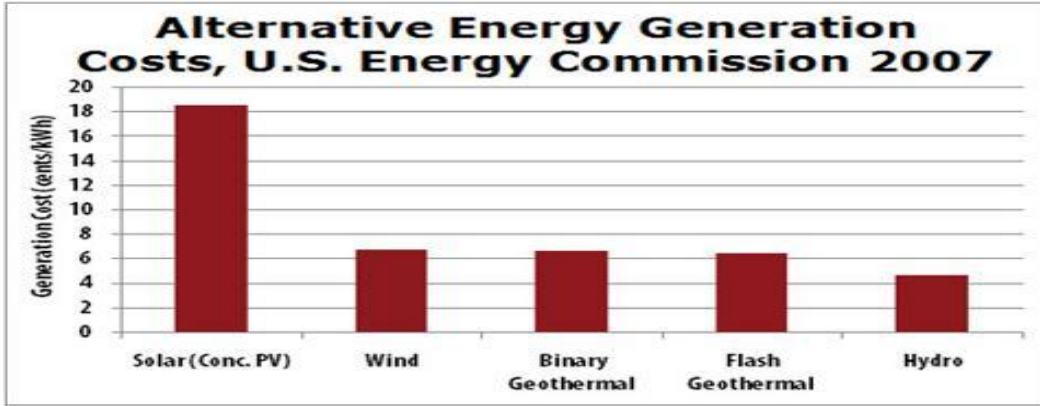


Fig. 2.2. Present price comparison of different renewable energy sources in cents/KW/h. [3]

Each of the plots indicates an exponential decrease. The wind, solar thermal are expected to drop to very low price around $.02/KW/h, but the solar PV is still around $.10/KW/h which is quite high compared to the present coal pricing.
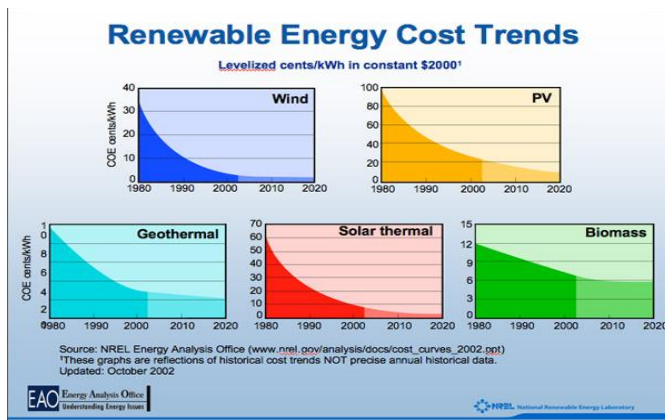


Fig. 2.3. Estimated drop in the production costs per KW/h for different renewable sources of energy. [4]

## 2.2 Photovoltaics

Imagine a device when under exposure to sun's radiation gives out electric current with no emissions, transmission losses or toxic residues, that is a photovoltaic device. It's a semiconductor device, which exhibits the photoelectric effect when exposed to sunlight. First observed by Alexandre-Edmond Becquerel in 1839 the photovoltaic effect can be defined as the creation of voltage or corresponding current in a device or material when exposed to light [5]. There is a very important point, which we need to point out her is the distinguishing factor between photoelectric effect and photovoltaic effect. Though both of them are directly related to each other, the phenomenon in each of them is completely different. According to photoelectric effect when a device is exposed to sufficient energy radiation electrons absorb this energy and leave the material to produce electric current. Whereas in a photovoltaic effect this energy absorbed by electrons makes them to transfer between bands that is from valance band to conduction band. The figure on the left indicates the electron–hole pair generated and also the transition of the electron into the conduction band on excitation thus exhibiting photovoltaic effect. The figure on the right shows the electrons leaving the material on exposure to radiation indicating photoelectric effect.
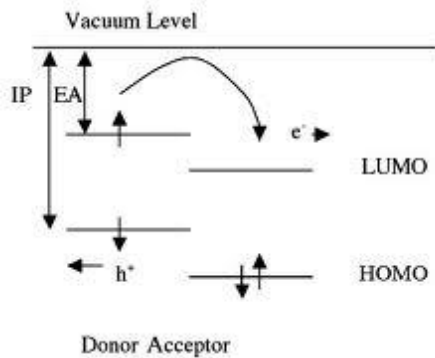
Fig. 2.4. Photovoltaic effect. [5]          Fig. 2.5. Photoelectric effect. [6]
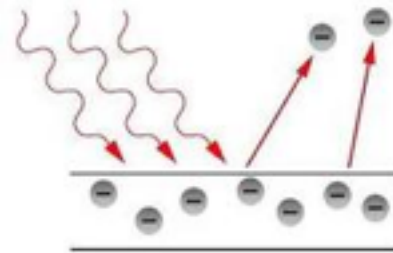
6

Such devices cannot just be laid open to expose them to sunlight, they need to be protected from environmental effects like rain, dust, animals and other external factors. Thus they are packed in modules behind glass sheets. The stacking up of these modules in series or parallel is based on the desired voltage and current outputs. We all know that when two cells are arranged in series the current remains the same but the voltage drop across each adds up, while the vice versa when arranged in parallel.

The operation of any photovoltaic device is based on a basic pn junction diode. It is very important that we have a clear understanding of what actually happens in the operation of a pn diode to understand the complexity we face in later chapters. A pn junction is a semiconductor with a p region and an n region attached closely to each other called the boundary junction. These regions are made out of a single semiconductor crystal rather than attaching two different crystals with different doping to be attached to each other because of the formation of grain boundaries. The doping can be done by various methods like Ion implantation, diffusion of dopants or bye epitaxy. An American physicist Russell Ohl at Bell laboratories first discovered this pn junction. Below is a block diagram showing both the p and n regions of the same crystal and the junction between the two, with no applied voltage across the terminals.
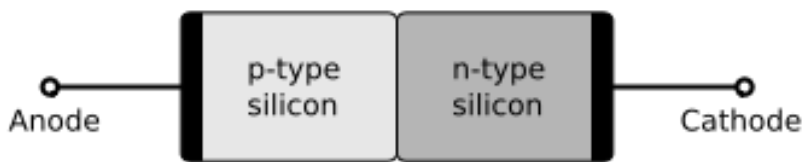


Fig. 2.6. A p-n junction diode without external voltage supply. [7]

Without an external applied voltage, when a p type and an n type are brought together to form a junction, the electrons near the p-n junction tend to diffuse into the p region leaving behind a positively charged ion also known as the donor in the n region. Same is the case when the holes near the p-n junction tend to diffuse into the n region leaving behind fixed ions also known as the acceptors in the p region. These electron and holes, which diffuse towards each other, are concentrated near the p-n junction because of which it loses its neutrality forming a space charge region also known as the depletion region. Due to this space charge region an electric field is developed across the junction, which opposes the further diffusion of electrons and holes towards the junction. Thus at the same time there are two phenomena which counteract and function at the junction. One is the diffusion of electrons and holes towards the junction and secondly the electric field, which counteracts this diffusion. Looking at the figure below would give a better picture of what we talked till now.
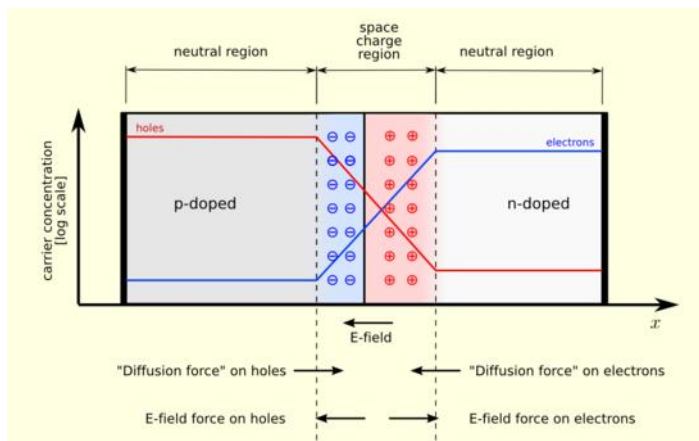


Fig. 2.7. A p-n junction diode in thermal equilibrium with zero bias voltage applied. [7]

The carrier concentrations at equilibrium are clearly indicated in the figure 2.7. The two counteracting forces tend to attain equilibrium. The figure below shows the plots

for space charge density, electric field and the voltage at equilibrium under zero external applied voltage.
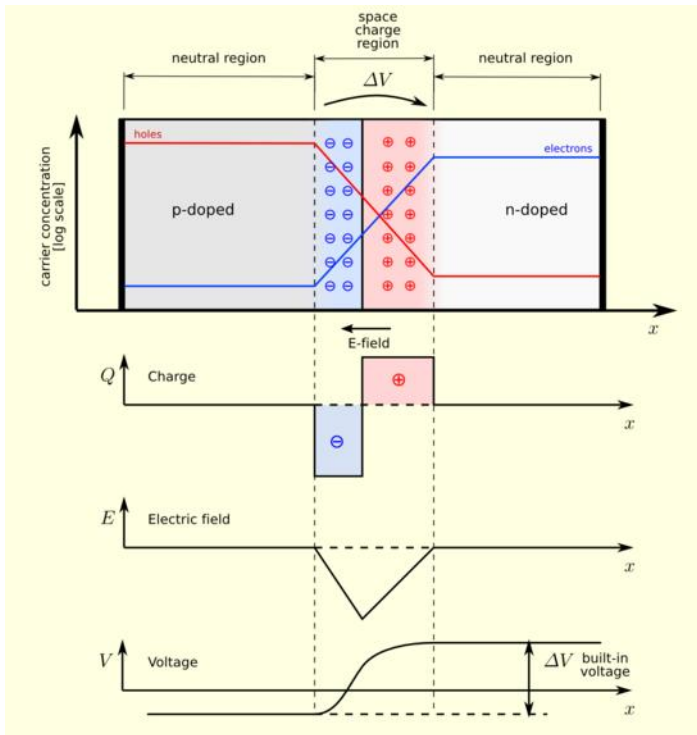


Fig. 2.8. A p-n junction diode in thermal equilibrium with zero bias voltage applied. Also shows plots for charge density, electric field and voltage. [7]

**2.2.1 Forward Bias**

In the forward bias the p region is connected to the positive terminal and the n region to the negative terminal of an external voltage source. When the voltage is applied the holes in the p region repel because of the positive bias and same is the case in the n region where the electrons are repelled by the negative bias. These electrons and holes diffuse towards the junction and lower the potential barrier at the junction. With the increase in the applied voltage in the forward bias the depletion becomes so thin that the electric field can no more counteract the diffusion phenomenon because of which

9

electrons tend to cross the junction into the p neutral region. Thus the amount of minority charge diffusing through the p region determines the amount of current flowing through the diode at a certain applied external voltage. In reality the electron penetration in the p region is only to a certain extent but this wouldn't affect the electric current, which remains constant all through out. This is because the holes drift in the p region towards the n region just as how electrons drift towards the p region. Any variation in the total current would create a charge build up with time according to Kirchhoff's current law.

### 2.2.2 Reverse Bias

This is just the opposite of a forward bias. Here the p region is connected to the negative bias of the external voltage source while the n region is connected to the positive bias as shown in the figure below.
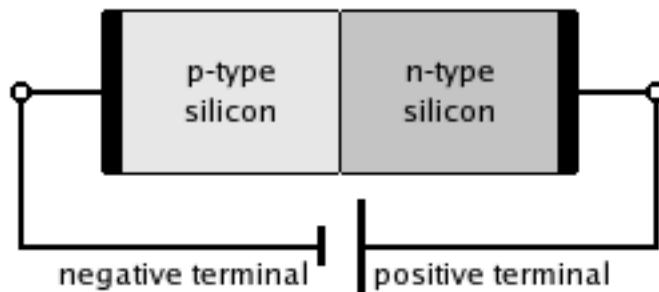


Fig. 2.9. A p-n junction acting in reverse bias under an external voltage bias. [7]

When a voltage is applied by the external voltage source across the terminals, the holes in the p region are pulled away from the junction into the negative terminal while the electrons in the n region are similarly pulled into the positive terminal. Thus the depletion region increases in width and keeps on going with the increase in the applied

10

voltage. This widening of the depletion region increases the resistance of the junction, which restricts the flow of electric current across the junction. The increase in resistance makes the diode work as an insulator in the reverse bias.

$$d = d_p + d_n = \sqrt{[(2\varepsilon/q)(N_A + N_D/N_A N_D)(V_{bi} - V)]} \text{ [7]}$$

The above equation gives d which is the total width of the depletion layer where $N_A$ is the acceptor concentration, $N_D$ is the donor concentration, $V_{bi}$ is the built in voltage, V is the external applied voltage, and $d_p$ and $d_n$ are the widths of the electric fields in p and n regions respectively. From this equation we can derive the built in voltage based on the equation mentioned below where T is the temperature of the substrate and K is the Boltzmann constant.

$$V_{bi} = (KT/q)\ln(N_A N_D/p_0 n_0) \text{ [7]}$$

Any technology, for it to be moved into a large scale productions is always reviewed on various factors like cost, efficiency, lifetime, its effect on the environment, etc. based on which photovoltaic energy is clean and green energy. There are no harmful byproducts nor does it emit any unwanted radiation, which makes it completely eco-friendly. These devices once installed in modules run for decades together with minimum maintenance costs or interventions. Thus the operating cost of PV technology is extremely low compared to other available technologies. The most important factor, which makes PV technology unique from others, is the availability of its input or source. Could be that we can't harness wind, hydro or other forms of energy at any place on earth but sunlight is something which is available everywhere. The earth receives 89,000 TW of sunlight, which is like 6000 times the 15 TW equivalent of the average power consumption of humans. These panels could be installed anywhere on the earth surface

which receives sufficient radiation from the sun. The panels are now being installed where ever possible like roof tops, moving cars, space satellites, and also in stationary devices such as water pumps, parking meters, temporary traffic signals and even remote guard posts and signals. A recent study on the possibility of laying panels on roadways is done on a 45 mile stretch roadway in Idaho, as roads are unobstructed from sunlight all the time and are one major section of land use.

Nothing is perfect and so is PV technology. It has its own disadvantages, which to some extent are possible to minimize. Firstly in a span of 24 hours any part of the earth on an average can receive sunlight only for 12 hours. Once it sets till the time it rises these panels don't have light to operate on. This disadvantage could be minimized to a certain extent by using batteries to store energy during the day, which could be used at night. Same is the case in a cloudy forecast. Photovoltaic panels are expensive to install. Though once installed it doesn't need much maintenance and runs for decades, the initial cost that goes into these panels is higher compared to other energy sources. There is a lot of research, which is presently going on around the world to reduce this cost.

The performance of the solar panels is greatly affected due to two reasons. Firstly the temperature of these panels should be maintained at room temperature. Above room temperature, their performance is dropped which is a major concern. Secondly to attain the best possible efficiency out of any device, the panels should be oriented normal to the sun's radiation. But because of the continuous disposition of the sun with respect to the panel, these panels are moved to follow the sun using solar trackers. It is observed that by using these solar trackers these panels see more sun by at least 30% in winter and 50% in

summer. Another disadvantage is that these panels produce DC, which needs to be converted to AC using inverters to meet the existing distribution grids.

## 2.3 Thin Film Technology

Before we get into detail on thin film technology we should first brief ourselves about what a solar cell is all about. A solar cell also known as a photovoltaic cell is a solid-state device that converts energy in the sunlight into DC current. The first solar cell was made at Bell laboratories in 1954 by Daryl Chapin, Calvin Souther Fuller and Gerald Pearson. These cells as we know are assembled in modules also known as solar panels. The best efficiency for Si till date is at 24.2% by Sunpower, a photovoltaic company based in San Jose. Though there is a lot of academic research going on around the world with lab efficiencies reaching 40.7% by Boeing spectrolab, efficiencies at industry scale are still limited to a market average of 12-18%.
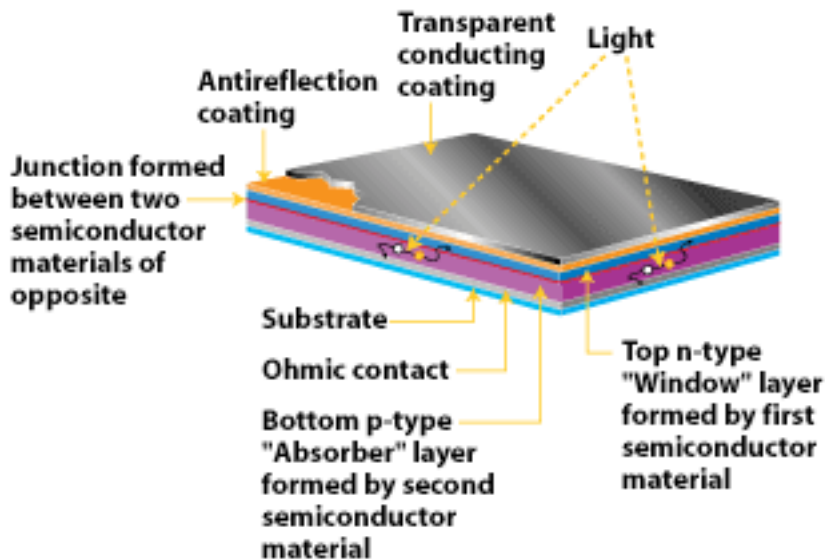


Fig. 2.10. A typical poly-crystalline thin film solar cell, which represents each layer deposited to form the final cell. [8]

The figure 2.10 shows the layer-by-layer deposition of a general thin film poly-crystalline solar cell. Layers of different materials are deposited one by one on a substrate. So we start off with the substrate, which can be glass, silicon, etc. Next comes the front contact, which is generally molybdenum, after which comes the actual layers of semiconductors. First come the p layer and then the n layer. The junction between the p and n layer is also been shown in the figure. Over them comes the antireflection coating, which consists of a thin layer of dielectric with a specific thickness. The coating helps in avoiding the sunrays hitting the cell from reflecting back. The interference effects in the coating cause the wave reflected from the antireflection coating top surface to be out of phase with the wave reflected from the semiconductor surface. These out of phase reflected waves destructively interfere with one and other, resulting in zero net reflected energy [9]. The final layer over the antireflective coating is the top contact. Typical metals used here are aluminum, gold, silver, etc. The figure below gives a better understanding of how the antireflection coating works.
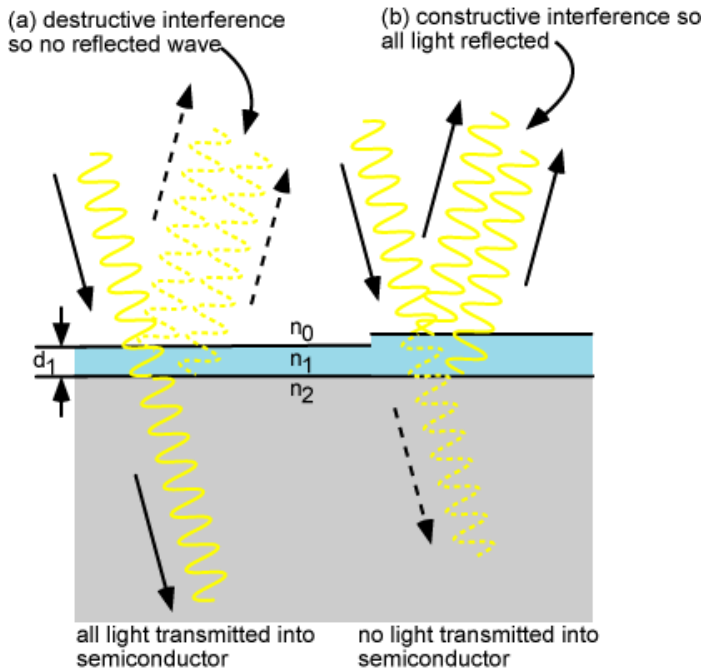
Fig. 2.11. Shows the constructive and destructive interference of light rays hitting an anti-reflective coating layer on a solar cell. [9]

Thin films solar cells (TFSC) also known as thin film photovoltaic cells (TFPC) are cells, which are made by depositing one or more thin layers of photovoltaic material on a substrate. The thickness of these cells varies from nanometers to micrometer range. There are numerous photovoltaic materials used in fabricating thin films. Even there are different substrates that are used like silicon, glass, and certain metals like aluminum. Most commonly used substrates used are wafer of single crystalline and polycrystalline silicon. Ingots are grown using Czochralski method or by controlled solidification of silicon in a crucible or mold. These ingots are then sliced into thin wafers by using fine saws of thickness above 150 μm. These wafer are then polished and processed till they are ready to be shipped to various companies to be made into solar cells. The high

material and processing cost makes it difficult for photovoltaic technology to reduce its KW/h price to drop below 10 cents.



Fig. 2.12. A typical silicon ingot grown using Czochralski method of various wafer sizes. [10]

The advantage thin films have over the silicon based industry re better throughputs, low material cost and less labor. Due extremely thin layers, adhesion to the substrate is a major concern. Few materials like Zinc don't stick to glass when deposited by chemical vapor deposition. We would discuss more in detail about it in later chapters. Other problems with thin films are the uniformity of deposition causing it to have various thicknesses even across small surface areas of substrates. At a laboratory level, cells could be produced with good quality, uniform thickness and composition producing good efficiencies. These are generally done on small substrates around a couple of square inches. But implementing the same technology on a larger substrate is a complete different ball game. All the factors mentioned above lead to macroscopic defects which effect the yield and the reliability of the cell based on its lifetime.

Based on the materials used thin films can be categorized into amorphous silicon (a-Si), Cadmium telluride (CdTe), Copper Indium Gallium Selenide (CIS or CIGS) and Dye-Sensitized solar cell (DSC). The figure 2.13 shows the various solar cell manufacturing technologies and where they stand as far as efficiencies are concerned. We can see that thin film technology is still evolving itself compared to the well-established silicon industry, which is far ahead thanks to the huge semiconductor industry, which accelerated the groundwork.
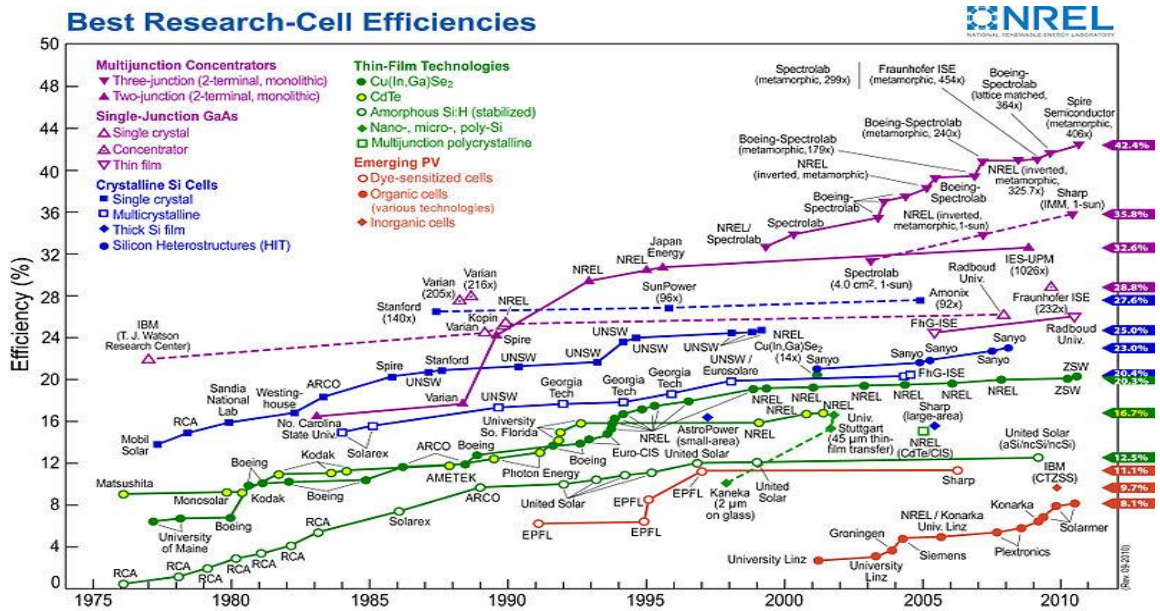


Fig. 2.13. Developments on the best research solar cell efficiencies in multi-junction, crystalline, thin film and other emerging PV technologies. [11]

This thesis is based on Kesterite ($Cu_2ZnSnSe_4$) absorber layer in which not much research has been done but is gaining lot of importance because of various factors, which would be discussed more in detail in the next section.

## 2.4 Kesterite Thin Film Photovoltaics

Copper indium selenide (CIS) and copper indium gallium selenide (CIGS) based thin film solar cells are well established and are at manufacturing level with highest efficiencies ranging around 20%. Due to scarcity of indium and gallium, these metals are getting expensive making the production costs to rise day by day. Indium and gallium are being consumed at unprecedented quantities for manufacturing LCD's for flat screen TV's. So how does one keep a track of how much of the metals are used up or how much is left before extinction? For a start the annual global consumption of the rare metals is not known in certainty [12]. Estimating the extractable reserves of many metals is also difficult. Such figure for indium and gallium are kept a closely guarded secret by mining companies. Governments and academia are only just starting to realize that there could be a problem looming, so studies of the issue are few and far between [12]. In a more detailed report, Reller has included the new projects and technologies and keeping all these in mind has projected that indium and gallium which are increasingly important in computer chips could be gone by 2017. The two pictures below gives a good understanding of all the rare metals and estimate of how long they might last. Also where are reserves of these valuable minerals present on the face of earth [12]?
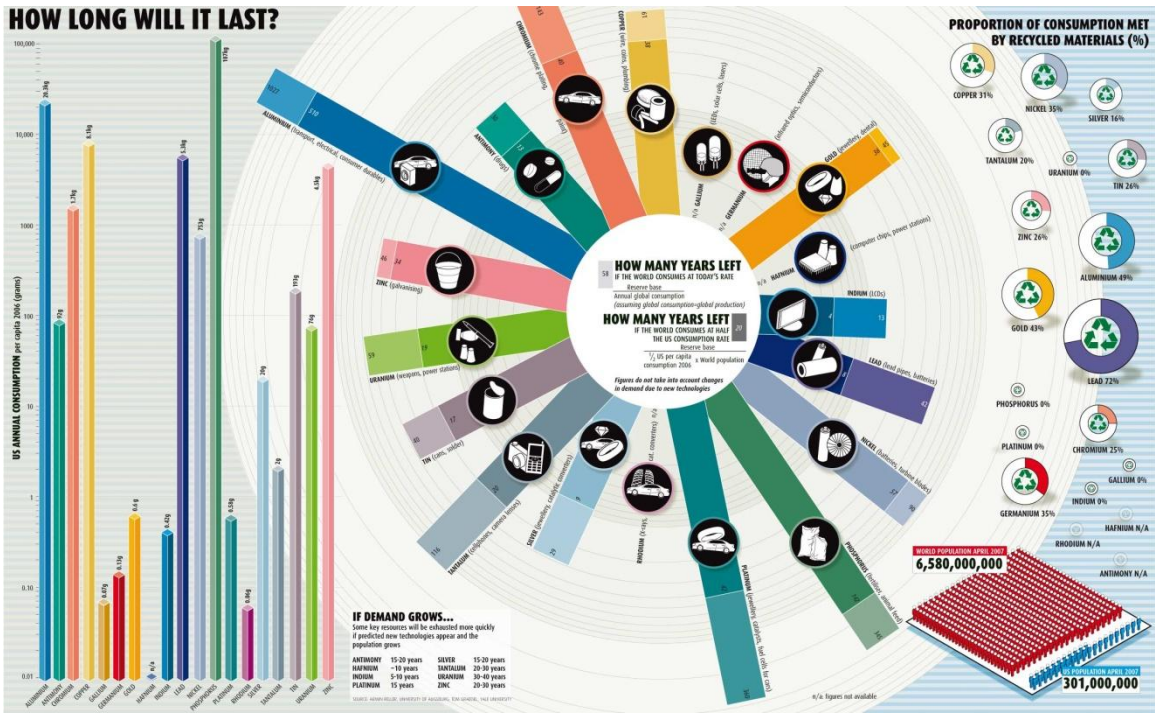
Fig. 2.14. Shows all the rare earth metals and how long they are expected to last before extinction. [12]
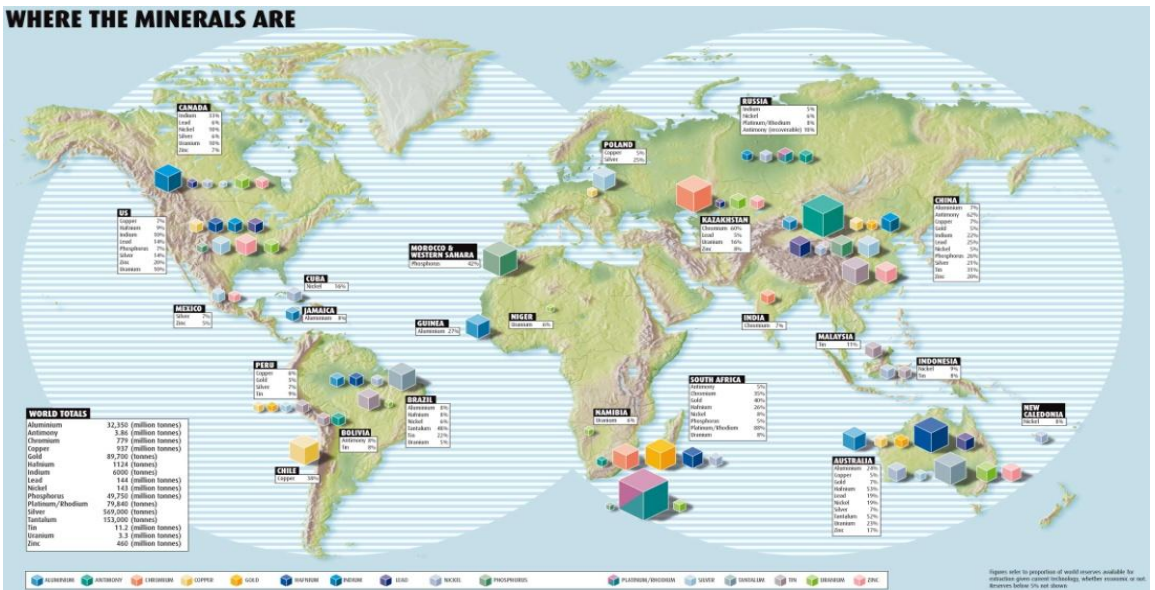


Fig. 2.15. A world map showing the reserves of all the rare earth elements. [12]

Researchers around the world are now on a look out to find metals that are a possible replacement to these elements. One such possibility is to replace indium with zinc (Zn) and tin (Sn). These metals are found in abundance and when properly replacing the indium lattice positions in the CIS crystal with zinc and tin we obtain the $Cu_2ZnSnSe_4$ crystal. CZSS as we call it also known as CZTSe is not much explored and the highest efficiencies obtained by many research groups around the world, is still limited at 5%.
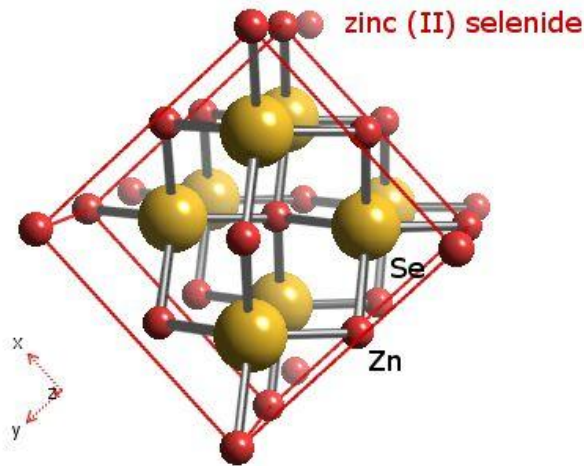


Fig. 2.16. ZnSe structure. [22]
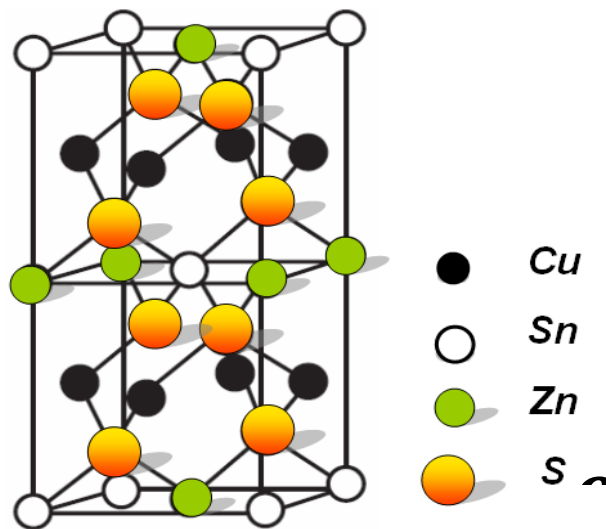


Fig. 2.17. CZSS structure. [23]

The ability of Kesterite selenide compound to be used as an absorber layer is verified but very little information is present to actually explain its optical properties and diffusion of metals during selenization step to synthesize the quaternary compound.

However there is a difference between CIS and CZSS absorber layers. Though CIS is proved to be an attractive material for photovoltaics, there are few properties of it, which are less than ideal, and on the other improved cell performance can be achieved by varying material properties as a function of depth. The advantage CIS films have is to alloy itself with other materials to attain desired material properties. In general for any given solar cell absorber layer, photons under the bandgap of the material are of no use in current generation. On the other hand we observe higher open circuit voltage for higher bandgap. Thus we can see there is a voltage-current tradeoff happening here. General studies convey information that the best efficiencies of any solar cells have bandgap around 1.4 and 1.5eV. As the bandgap of a good CIS film is around 1.0eV it could be alloyed with materials with high bandgap. When alloying two semiconductor materials the bandgap of the alloy tends to be a linear function of its composition [6]. The best-fit alloy for CIS is $CuGaSe_2$. Thus it was observed that by varying the gallium concentration we could actually have a wide range of bandgap's for CIS now a CIGS absorber layer. But with CZSS films there is no confirmed data as to what its ideal bandgap is. There are assumptions that because it is the same as CIS because we are trying to replace Indium with Zinc and Tin, even the bandgap also should be around the same.

## 2.5 Research Background

The best efficient solar cell based on Kesterite absorber layer is made by G Zoppi at Northumbria Photovoltaics Applications Centre. The band gap of their material is reported to be 0.8 eV for the Kesterite selenide material. The deposition procedure of fabrication involved sequential deposition of high purity elemental targets of Copper, Zinc and Tin through sputtering. After which the stack of metals were selenized at a high temperature to synthesize Kesterite material.

The CZSS material was produced by a two-stage process. The Cu, Zn and Sn were sequentially sputtered using high purity (5N) targets onto unheated molybdenum coated soda-lime glass substrate. The substrate is rotated in a substrate table to improve the step coverage. For better intermixing of the individual metals, a large number of alternate layers were used, each a few nm thick. Once the stack of metals is made, it is then selenized at 500 degrees centigrade for 30 min in the presence of argon and elemental selenium. The final thickness of the sample was adjusted to be 2 μm. The cell is completed y depositing CdS layer by chemical bath deposition method after which i-ZnO is deposited with a thickness of 50nm. Followed by which indium tin oxide is deposited using RF sputtering. Finally the contacts of Ni/Al are laid using sputtering. Once the samples were made they were tested for their optical and compositional properties. X-ray diffraction was used to determine the precursor materials and also for the structural quality of the sample, the film composition and morphology was observed using data from the technique electron diffraction spectroscopy in a scanning electron microscope. Elemental depth profiling gave the intensity of each element as a function of the depth [13].
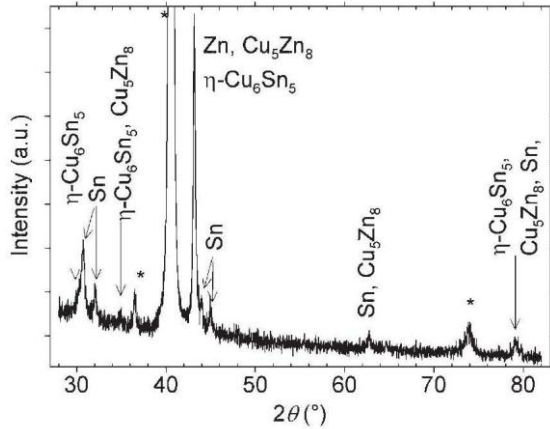
Fig. 2.18. XRD pattern of just the metal precursors Cu, Zn and Sn with Cu/(Zn+Sn)=0.85 and Zn/Sn=1.08 deposited on a moly coated soda lime glass. [13]

The plot above shows the XRD on well-mixed copper, zinc and tin metals before selenization step. The metals were deposited such that the ratio (Cu/(Zn+Sn)=0.85), making it Cu poor material. Also the Zn/Sn ratio is kept at 1.08 making Zn rich as compared to Sn [13]. These results were confirmed using the electron diffraction spectroscopy results, which give the composition of the individual elements. The plot shows binaries of Cu, Zn and Cu, Sn but no evidence of any binaries of Zn and Sn [13].
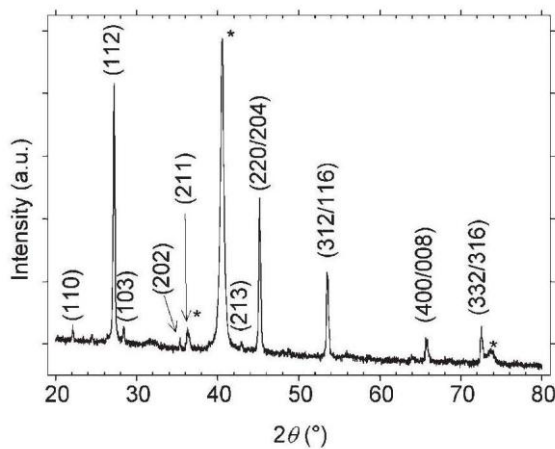


Fig. 2.19. XRD pattern of a CZSS film selenized at 500°C for 30 mins. Peaks marked (*) read silicon peaks from the substrate. [13]

23

After selenizing the metal stack at 500 degrees centigrade for 30 min they observed that the metal ratios were still remained the same. The plot above is an XRD on the sample after selenization. All the peaks shown are associated with the Kesterite material except for the * marked which came from the substrate. They confirm referring to previous stated data that the selenized film forms the stannite structure [13].
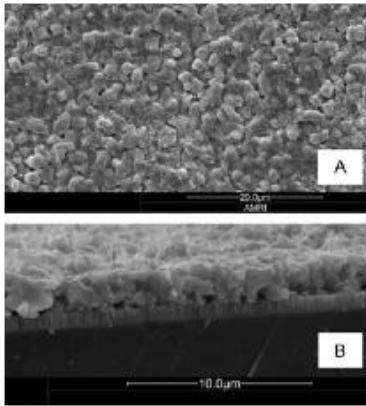


Fig. 2.20. Scanning electron micrograph of a CZSS film on a moly coated glass. (a) Surface image and (b) cross-sectional image. [13]

The surface image and cross sectional images were taken using scanning electron microscope. The grain width was observed to be 2 μm, which is the same as the thickness of the absorber layer [13]. This helps in maximizing both the minority carrier diffusion length and the built in potential in a polycrystalline thin film absorber layers. The depth profile of the individual elements in the sample reveals uniformity for both Sn and Se but traces of excess Cu were observed at the moly interface, reason they say is because Cu is deposited first on molybdenum. Even they observe a dip in the zinc in the middle of the sample. The figure below shows the depth profile of the CZSS film deposited on glass.
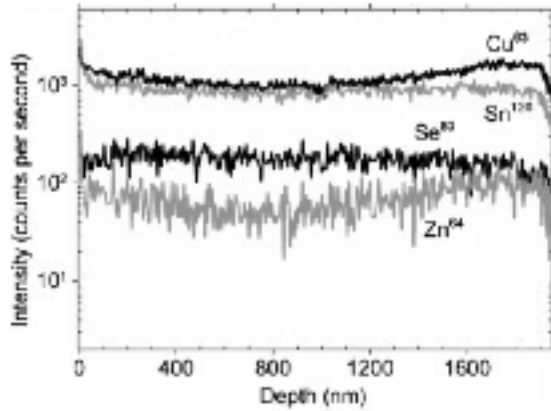
Fig. 2.21. Depth profiling of a CZSS film on glass done at 500°C for 30 min. [13]

There have been many discrepancies of the reported bandgap of the Kesterite thin films. Different research groups around the world have proposed different figures like 1.0 eV, 1.5 eV, etc. SeJin Ahn a Korean researcher feels that films prepared by co-evaporation of Cu, Zn, Sn and Se at a substrate temperature of 370 degrees centigrade would yield a bandgap of 1.0 eV irrespective of the method used to obtain the bandgap [14]. He also postulates with proven results that as we gradually increase the substrate temperature to 500 degrees centigrade the bandgap increases because of the formation of ZnSe at the CZSS/moly interface. Due to the uncertainty about the bandgap value it was felt that the method one uses to determine the bandgap would greatly affect the bandgap itself.

The samples were prepared in a single stage co-evaporation technique on a soda lime glass using Knudsen-type effusion cells as evaporation sources at micro torr pressure conditions for optical measurements [14]. The same layer was also developed on a soda lime glass substrate with 1 μm thickness of molybdenum. For external quantum efficiency (EQE) measurement to determine bandgap of the material thin film cells were

fabricated by growing the n layer of CdS buffer layer of thickness of 60nm. Over that an i-ZnO of 50nm and Al doped n-ZnO of 500nm were deposited by RF magnetron sputtering. An Al grid of 500nm in thickness was deposited as a current collector using thermal evaporation [14].

The composition and morphology were observed using a scanning electron microscope and energy dispersive spectroscopy (EDS). The crystal structure determination was done y using X-ray diffraction (XRD) and Raman spectroscopy and the depth compositional profiling was done by using Auger electron spectroscopy (AES). In order to clear the discrepancies on the bandgap three techniques were used to obtain $E_g$ value. Transmission measurements, PL measurements and external quantum efficiency (EQE) by using an incident photon conversion efficiency (IPCE) measurement unit [14].

In the figure below, we can see the cross sectional and plane view SEM micrographs of the sample prepared at a substrate temperature of 370 degrees centigrade. The pictures indicate a well facetted grains of 2.6 μm are formed. Part (c) and (d) of the figure display the XRD and Raman spectra, which indicate that the synthesized film is apparently a phase pure CZSS material without any secondary phases. The composition of the film through EDS analysis is derived to be Cu/(Zn+Sn)= 0.82, Zn/Sn= 1.15 and Se/metal=1.04.
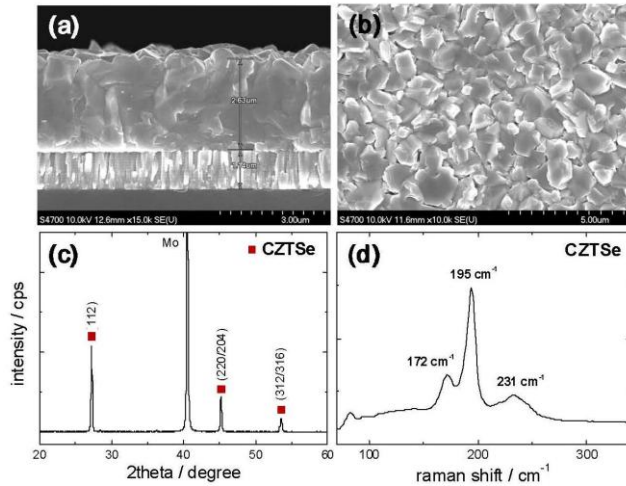
Fig. 2.22. SEM micrographs of film deposited at 370°C. (a) Cross-sectional and (b) plane view (c) XRD pattern (d) Raman spectra. [14]

The various techniques to determine $E_g$ were done and the obtained plots are shown in the diagram below. The transmission was performed on a wavelength range of 200-1800nm by means of a UV-VIS-NIR spectrophotometer and the hν vs $(αhν)^2$ plot is shown in part (a) [14]. For the EQE analysis to determine $E_g$, the relation $[hν×ln (1-EQE)]^2$ vs hν was done and shown in part (b). Part (c) shows the PL measurements of the bandgap. Thus the author says irrespective of the method used to determine the bandgap, the value obtained is around 1 eV.
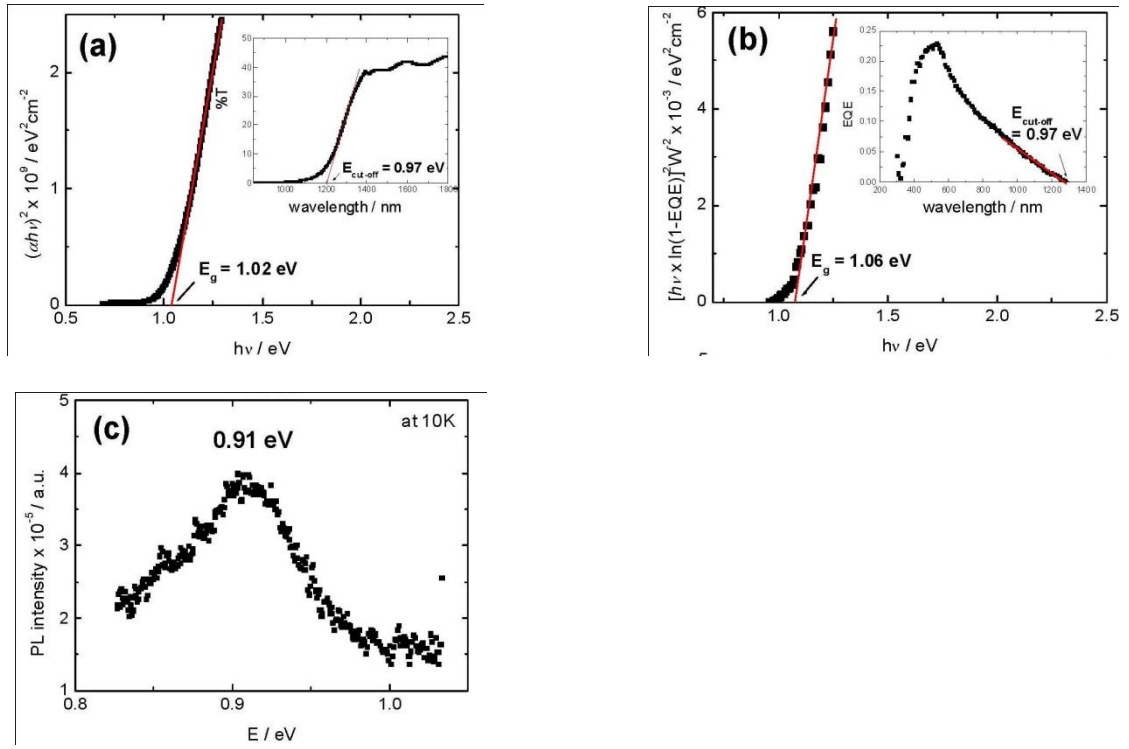
Fig. 2.23. Determination of $E_g$ value by (a) Transmission (b) EQE (c) PL measurements. [14]

Samples were now done at varying substrate temperatures ranging from 320 to 500 degrees centigrade. The figure below shows the comparison of these different samples based on the transmission, $E_g$ values and the XRD pattern.
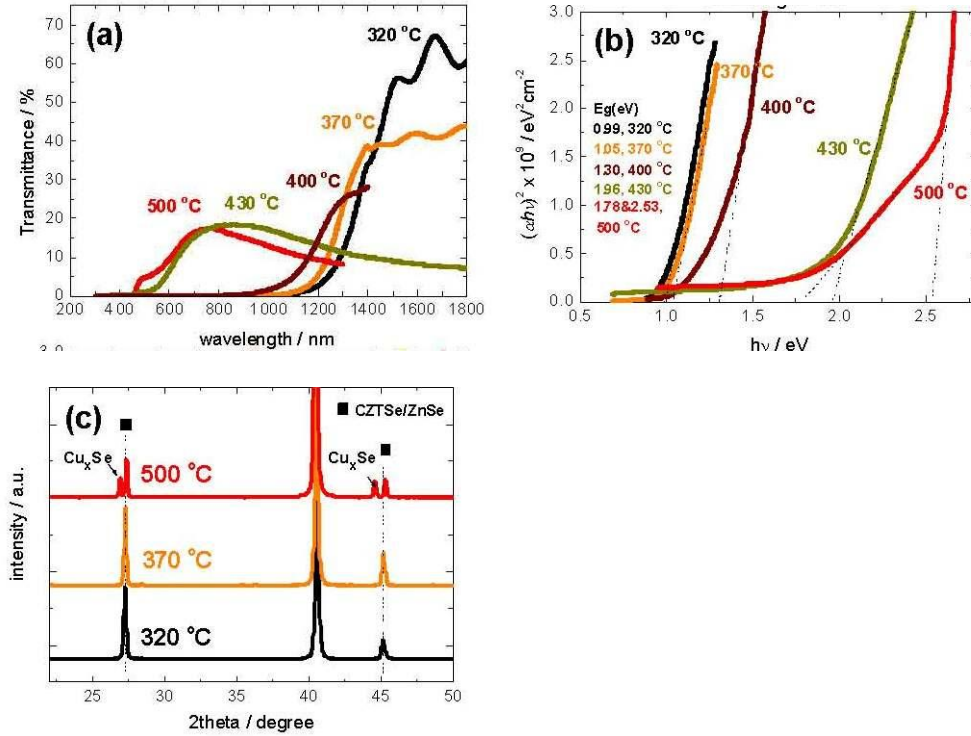


Fig. 2.24. (a) transmission data (b) $E_g$ values and (c) XRD patterns observed for various substrate temperatures. [14]

If we look at the plot (b), which shows the $E_g$ at different substrate temperatures, we see a gradual increase. Just in the difference from 320 to 400 degrees centigrade, we observe a significant change in $E_g$ from .99 to 1.3 eV [14]. Using Auger electron spectroscopy the depth profile of the films reveal that the film done at 320 degrees centigrade showed uniform distribution of elements throughout the entire film depth, while from substrate temperatures higher than 370 degree centigrade, the segregation of Zn and Se at CZSS/moly interface was clearly observed [14]. This is believed to be ZnSe,

29

and its fraction is observed to increase with the increase in substrate temperature [14]. Thus based on the previous statement it is now clear that the discrepancies over the actual value of the bandgap arise not because of the method implemented in finding out $E_g$, but because of the formation of ZnSe based on the substrate temperature. The sample done at 500 degrees centigrade shows a bandgap of 2.5, which could be related to the bandgap of ZnSe. This proves that ZnSe is excessively present in this sample. Thus as the substrate temperature increases the amount of ZnSe in the sample increases because of which the bandgap increases. The second interesting fact observed is in the XRD spectra. All the XRD plots look the same and show no difference based on the material formed to distinguish between CZSS and ZnSe. Understanding of the $2\theta$ values of these individual materials it was found that the peaks exactly coincide [14]. Thus they could conclude the fact that XRD isn't the correct analysis to determine the crystal structure, which may mislead us, and any complementary tool is needed [14].

The procedure followed in depositing the metals either by co-depositing or sequentially has proved to have distinguishing effect on the morphology and the precursors obtained after annealing the sample. The effects of different orders in which the metals were deposited on the properties of the film are well studied by O. Volobujeva at Tallinn University of Technology. He deposited metals in different orders and selenized them through a range of substrate temperatures to study the composition, morphology, and precursor formation at each range [15]. Precursor films with a different sequence of metals Cu, Zn and Sn were deposited on a soda lime glass substrate through vacuum evaporation [15]. The two parameters he used in his study to distinguish the films formed were based on the order of metal deposition and the selenization

30

temperature. The thickness of individual elements was controlled by using quartz crystals, which monitor the evaporation time, and also through scanning electron microscope. Given below shows the deposition process of the precursor films. Once the stack of metals is made elemental Se was used to selenized and form the absorber layer using isothermal sealed quartz ampoules [15]. The Selenization was done through a range of 210 to 550 degrees centigrade for duration varying from .25 to 2 hours. Once the sample were done the surface morphology and crystalline structure were studied using high resolution scanning electron microscope, the chemical composition and stoichiometry were analyzed with energy dispersive x-ray analysis and the bulk structure and phase compositions were studied using X-ray diffraction and Raman spectroscopy [15].

Table 2.1. Deposition process parameters of precursor CZSS film. [15]

| | Sequence of layers | Substrate, temperature, $^0C$ | Composition of precursor films |
|---|---|---|---|
| 1 | Sn-Cu-Zn | 150 | (Cu/Zn)=1.8 <br> Zn/Sn=1.2 <br> Cu/(Zn+Sn)=1.0 |
| 2 | Zn-Cu-Sn-Zn- Cu-Sn | 120 | (Cu/Zn)=1.4 <br> Zn/Sn=1.8 <br> Cu/(Zn+Sn)=1.9 |
| 3 | Cu-Zn-Sn | 150 | (Cu/Zn)=2.7 <br> Zn/Sn=0.9 <br> Cu/(Zn+Sn)=1.3 |
| 4 | 2Cu/Sn-Zn | 150 | (Cu/Zn)=1.9 <br> Zn/Sn=0.95 <br> Cu/(Zn+Sn)=0.9 |
| 5 | 2Cu/Sn-Zn- 2Cu/Sn-Zn | 150 | (Cu/Zn)=1.9 <br> Zn/Sn=0.9 <br> Cu/(Zn+Sn)=0.95 |

The author feels the sequence in which the metals are laid out greatly influences the morphology of the precursor films. Study on Sn-Zn-Cu precursor films were performed and SEM images indicate a "mesa-like structure " uniformly extended throughout the film till the moly interface. He feels that the non-uniform Sn deposition forming discontinuous layer of semispherical crystals on the moly is the reason behind this crystal structure. This discontinuous Sn deposition is also observed when Cu-Zn-Sn was deposited in the order specified, which confirms the same crystal structure. The images of both these samples are shown below [15].
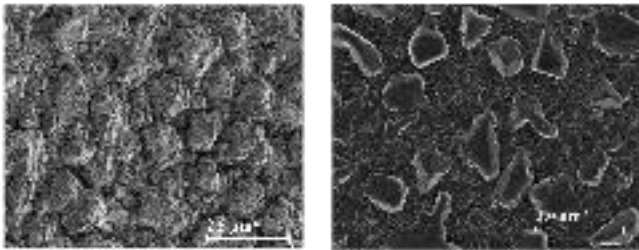


Fig. 2.25. SEM micrographs of the surface of films fabricated in the order (a) Sn-Zn-Cu (b) Cu-Zn-Sn. [15]

The XRD on theses samples gives evidence of alloy formation between Cu-Sn and Cu-Zn, which are shown in the figures below. Peaks of $Cu_6Sn_5$ and $Cu_3Sn$ forms in the samples give a Cu/Sn ratio of 2:1 as shown in the figure [15].
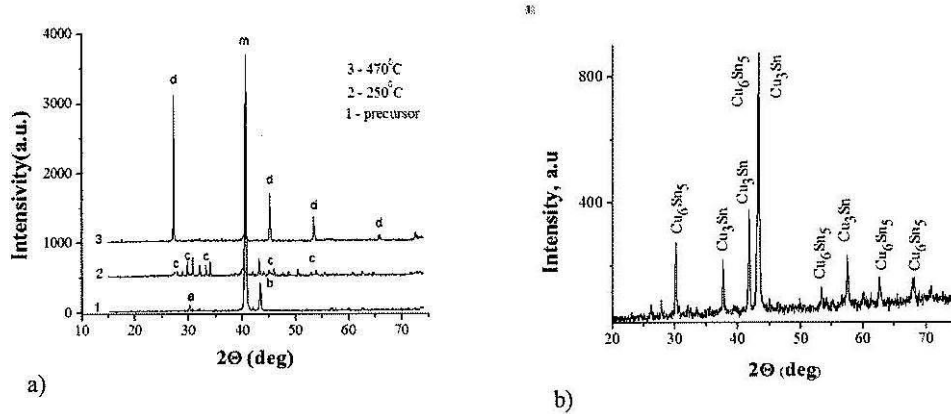


Fig. 2.26. XRD patterns of (a) (1) precursor metals Cu-Zn-Sn film, (2) selenized at 250°C, (3)at 470°C. Peak Identification: a- $Cu_2Sn_5$, b- $Cu_5Zn_8$, c- $CuSe_2$, d-$Cu_2ZnSnSe_4$, m-Mo.(b) XRD pattern showing alloy of 2Cu+Sn layer. [15]

Another order of deposition explored by them is the 2Cu/Sn-Zn and 2Cu/Sn-Zn-2Cu/Sn-Zn, where co-deposition of Cu and Sn was done forming an alloy with a ratio of 2:1 atomic percentage instead of sequentially depositing them. The obtained films were smoother and uniform all throughout as compared too the previously made sample of different order. Selenization of these samples at substrate temperature 250 degrees centigrade and analyzing their morphology indicates a closely packed agglomerated formation with crystals in a sub micron size (50-100nm) [15]. The comparison of these two different types of crystal formation based on the order of deposition is clearly shown in the figure below.

33
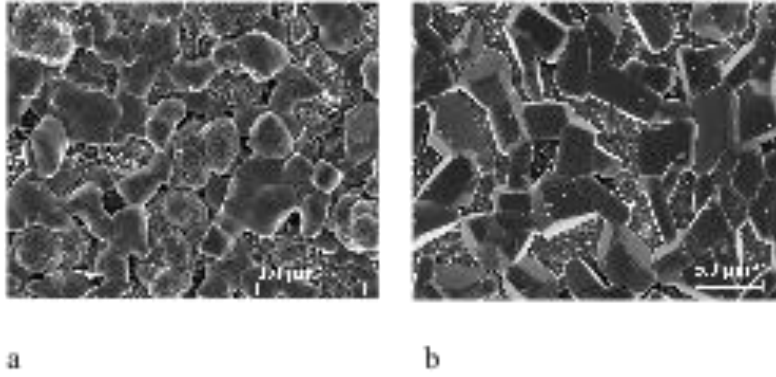
Fig. 2.27. SEM micrographs of (a) Sn-Zn-Cu films at Sub Temp. 250°C and (b) Cu/Sn-Zn film surface selenized at Sub. Temp. 300°C. [15]

When the same samples are synthesized at a substrate temperature of 300, the EDS analysis clearly indicates the formation of CuSe [15]. Also the inner particles in the sample show a ternary mixture of CZSS, $Cu_2SnSe_3$ and ZnSe phases. The author felt that the presence of CZSS in the film is based on the order implemented as the samples done in the order Sn-Zn-Cu has no phase indications of CZSS but @Cu/Sn-Zn did [15]. He also felt that as the substrate temperature increases the amount of ternary $Cu_2SnSe_3$ decreases and eventually stops in samples done above 400 degrees centigrade [15]. This is shown in the figure below.

The structure of these samples made at substrate temperature higher than 420 degrees centigrade still retains its two-level structure; sparse packed large crystals in sizes of up to 1-2 μm at the surface layer and dense small-crystalline bottom layer with sizes around 50-200 nm [15]. Better efficiencies are observed for films having bigger grain structures but also the presence of CuSe on the surface and also inside the films are very much evident which reduces the efficiency in these films.
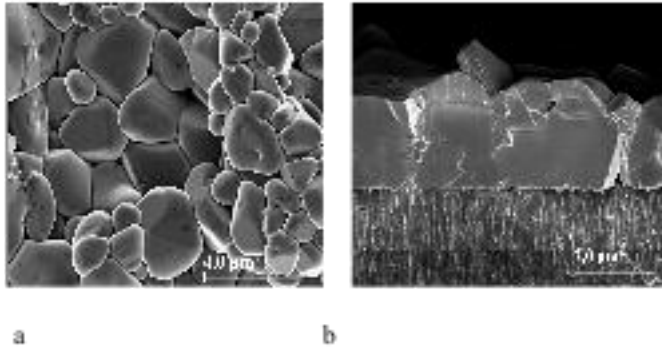
Fig. 2.28. SEM images of the surface of a stoichiometric film done at Sub. Temp. 470°C. (a) cross-section (b) Cu rich precursor film selenized at 470°C. [15]

A review of literature done by Phillip J. Dale gives a comparison of the optical and characteristic properties of different types of absorber layers. The comparison gives us a good understanding of the differences in the best efficient chalcopyrite and Kesterite (S/Se) films along with CIGS plots. The author himself synthesized Kesterite sulphide film by first stacking metals on a molybdenum coated soda lime glass in the order Cu-Sn-Cu-Zn using electro-deposition method. The precursor stack is then annealed in the presence of elemental sulfur in 0.5 bar forming gas. Devices were then completed by sequentially depositing CdS using chemical bath deposition, unintentionally doped zinc oxide (i-ZnO), aluminum doped zinc oxide (Al-ZnO) and Ni-Al metal contacts. Given below is a comparison based on current voltage curves for chalcopyrite (S/Se) and Kesterite (S/Se) absorber layers.
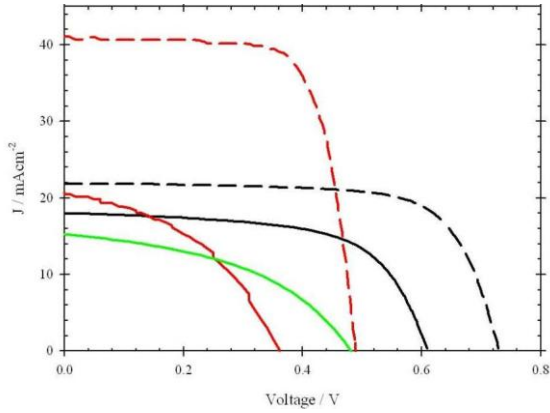
Fig. 2.29. I-V curves for the best efficient $Cu_2ZnSnS_4$ (Black), $CuInS_2$ (Black dash), $Cu_2ZnSnSe_4$ (Red), $CuInSe_2$ (Red dash) and EDA- $Cu_2ZnSnS_4$ (Green). Data adapted from references [17, 13, 18, 19]. [16]

The Kesterite sulphide has an open circuit voltage $V_{oc}$ of 610mV, which is 120mV less than its chalcopyrite counterpart. This could be because of the difference in the bandgap values of each of these materials. Studying figure 2.29 we can determine the bandgap of chalcopyrite sulphide to be 1.46 and 1.36 for the record Kesterite sulphide. Similarly the short circuit current $J_{sc}$ of the best Kesterite sulphide is 17.9 mAcm$^{-2}$, which is 4 mAcm$^{-2}$ less than chalcopyrite sulphide. Coming to the chalcopyrite and Kesterite selenide samples, the examination of the EQE curves shows that the chalcopyrite cell generates extractable carriers almost perfectly over a wide wavelength range. Whereas the Kesterite device has a lower maximum collection efficiency of around 60%. Kesterite selenide has worse fill factor than the Kesterite sulphide device, and a lower $V_{oc}$ leading to a lower overall device efficiency. The corresponding parameter data of each of these devices is shown in table 2.2.

Table 2.2. Parameters of best Kesterite and Chalcopyrite devices [17, 13, 18, 19]. [16]

| Device | $V_{oc}$ / mV | $J_{sc}$ / mA cm$^{-2}$ | FF / % | $\eta$ / % | $R_p$ / k$\Omega$ cm$^2$ | $R_s$ / $\Omega$ cm$^2$ | A / cm$^2$ |
|---|---|---|---|---|---|---|---|
| Katagiri 08 | 610 | 17.9 | 62 | 6.77 | 0.37 | 4.25 | 0.15 act |
| Siemer 01 | 729 | 21.8 | 72 | 11.4 | - | - | 0.51 |
| EDA-CZTS | 480 | 15.3 | 45 | 3.3 | 0.13 | 1.8 light | 0.24 |
| Zoppi 09 | 359 | 20.7 | 43 | 3.2 | 0.11 | 3.9 | 0.23 |
| Abu-shama04 | 491 | 41.1 | 72 | 14.5 | - | - | 0.45 |
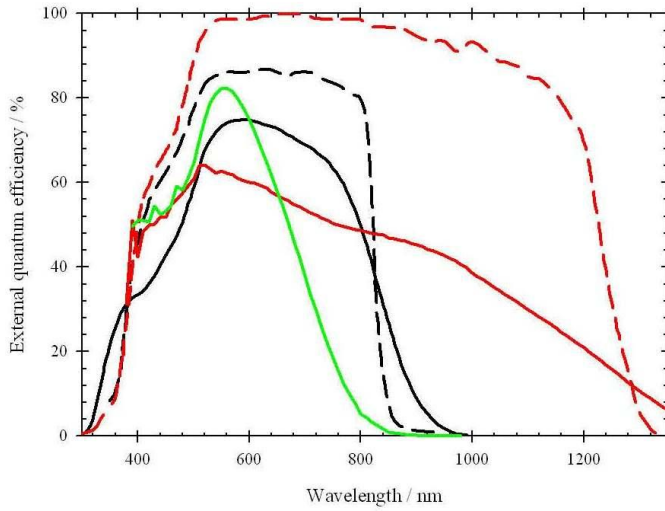


Fig. 2.30. EQE curves of the best efficient $Cu_2ZnSnS_4$ (Black), $CuInS_2$ (Black dash), $Cu_2ZnSnSe_4$ (Red), $CuInSe_2$ (Red dash) and EDA- $Cu_2ZnSnS_4$ (Green). Data adapted from references [17, 13, 18, 19]. [16]

The objective of any researcher working on solar cell absorber layers is to form a film with no secondary phases. But unfortunately due to the complexity of the quaternary Kesterite compound the margin of error is very large. The X-ray diffraction is used to determine the phase composition of the Kesterite sulphide material. The Katagari group

did not find any secondary phases using XRD but the EDA Kesterite sulphide as shown in the figure 2.30 did show secondary phases. Even they were surprised to find out that the peaks for $CuSnS_3$ and ZnS coincide with the main reflexes of the quaternary compound. But the presence of $Cu_2ZnSnS_4$ is confirmed by other minor reflexes which do not overlap with the secondary phases. Thus they conclude that by just using XRD alone, we cannot determine the phase composition of this material, which is the same with the Kesterite selenide material mentioned before.
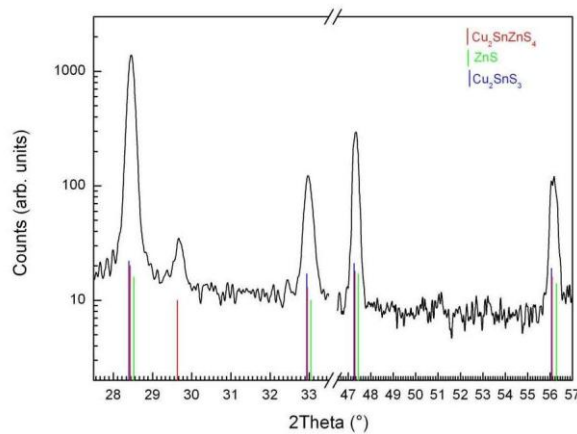


Fig. 2.31. XRD grazing incidence diagram with reference $Cu_2ZnSnS_4$, $Cu_2SnS_3$ and ZnS peaks. Marked JCPDS 01-075-4122, 01-071-5975,00-027-0198 respectively. [16]

Thus now that we have done a review of works of different research groups around the world who are working on Kesterite based absorber layers, we get an understanding of the parameters affecting, the challenges faced and the methods implemented to overcome these challenges. The bandgap of this material is still not known for sure. Each of the groups came up with different values varying from 0.9 to 1.5 eV with their individual proven results but there is not one value, which they could all agree upon. Thus determining the actual bandgap value of this material would be an

important task in my research. Secondly, the methodology of each of these groups is different. Few groups used co-evaporation, few stacked up metals before selenization and few used precursor materials and also alloy formation. Determining the best possible method to produce films with good uniformity, morphology and the right grain structure would be of utmost importance, not to forget the stoichiometry. In this study we looked into the problem of films having multiple phases other than CZSS like ZnSe, CuSe, $Cu_2SnSe_3$, etc. Thus forming a quaternary absorber layer involving four elements to form one compound all being in a single phase would definitely be a complex and challenging task. Also to keep in mind the ZnSe layer formation at the CZSS/moly interface, which cannot be distinguished from CZSS in XRD measurements is very important. The loss of Sn when operating the substrate temperature above 420 degrees centigrade is a major concern.

In the next chapter, the methodology is described in detail, as well as the modifications to correct certain defects encountered, the equipment to fabricate each layer of the solar cell and the characteristic and optical measurements done on the samples.

## 3. EXPERIMENTAL APPARATUS AND PROCEDURE

In this chapter I would be explaining in detail the design and operation of each component of the apparatus used in fabrication of the Kesterite (CZSS) based p type absorber layer and all the other layers being deposited to form the final solar cell. I would then explain the step-by-step procedure followed till the final sample is prepared. After which I shall give an overview of the material and device characterization techniques and the equipment involved in this study.

### 3.1 CZSS Deposition Apparatus

The CZSS Kesterite compound is deposited using physical vapor deposition technique. The chamber is designed specifically in such a way that each individual element or multiple elements simultaneously could be controllably deposited on to a substrate at a desired rate. The apparatus is equipped with isolated elemental effusion sources also known as a gun whose temperature is controlled using a power controller. The real time temperatures of these guns could be observed by installing individual thermocouples which sense the temperature compared to the set value on the power controller. As we operate the procedure at micro torr ($10^{-6}$ torr) we equip the chamber with a mechanical pump which pumps down to milli torr ($10^{-3}$ torr), after which the turbo pump takes charge and pumps the chamber down to micro torr range. We use pressure

gauges for both the mechanical and turbo (ultra high vacuum) pumps like ion gauges. After the desired pressure is read, the process of deposition starts. A schematic of the chamber is shown in figure 3.1 and 3.2.

The equipment I used for physical vapor deposition consists of two isolated chambers each holding two guns, named chamber 1 and chamber 2. Chamber 1 holds Copper and Tin guns while chamber 2 hold Zinc and Selenium. Each of these chambers is well equipped and is designed to function in a similar fashion. The gun has an inner shield and outer shield to block the radiations emitted from the heated coil. The coil is made of tantalum wire, which is in a cylindrical fashion surrounding the elemental source material. The source is laid in a liner made of molybdenum or tantalum, which is put in a crucible generally made of quartz or ceramic, which insulates the liner from the chamber to avoid shorting. An arrow marked towards the gun indicates the leads from the power controller going to the gun through which the current passes. The leads are insulated using small ceramic pieces all along its path to avoid these shorts to the chamber. Contaminated ceramics are replaced time to time to avoid uncontrolled deposition. The thermocouple implanted for each gun reads the real time temperature of the gun and which is sent back to the power controller and is comparable to the already set temperature value in the controller. Similar to the leads mentioned above the thermocouple is also covered with insulating material to avoid shorts or formation of secondary thermocouple along its circuitry path to the gun and back. The arrow pointing back towards the power controller indicates this action.
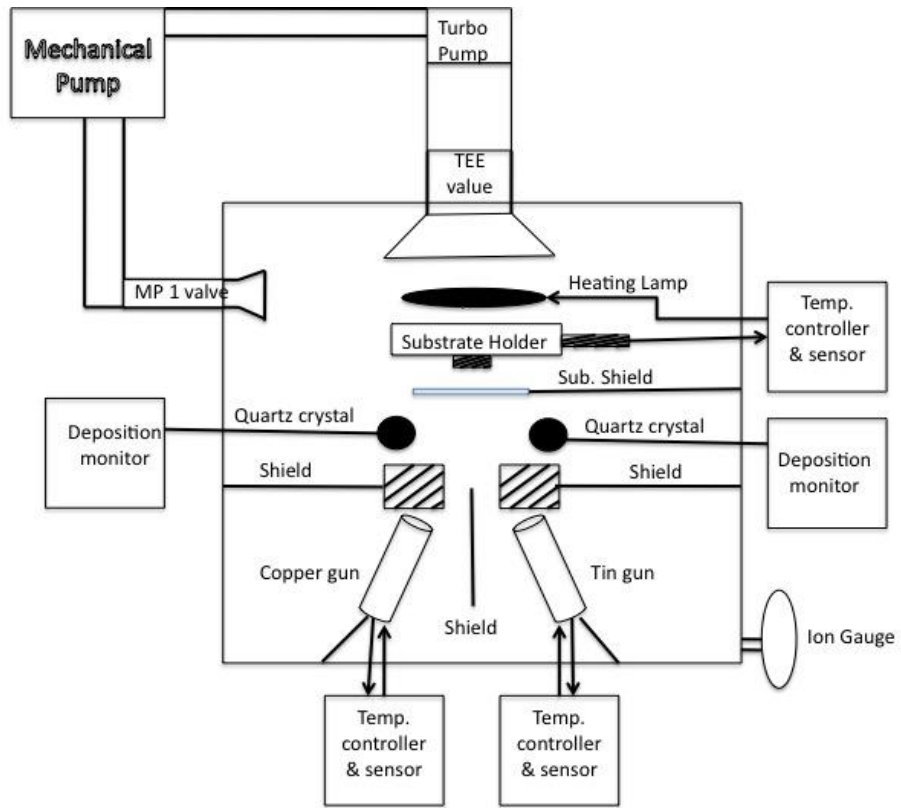
Fig. 3.1. Schematic of chamber 1 with copper and tin elemental sources.
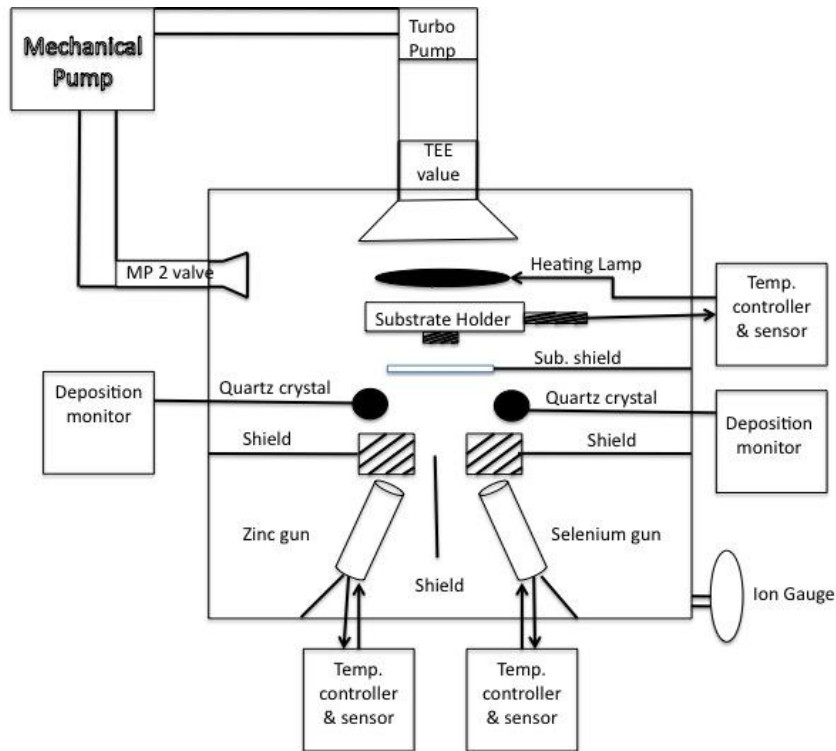
Fig. 3.2. Schematic of chamber 2 with zinc and selenium elemental sources.

Each gun has its own quartz crystal, which is used to measure the flux rate of that particular element. The Crystal holder holds a gold-coated crystal sensor. The Reading from the senor is indicated on a deposition monitor, which displays the rate of deposition, thickness of the material deposited and the time duration for which the deposition occurred. The way it operates is based on piezoelectric sensitivity of a quartz monitor crystal to added mass. The quartz crystal microbalance uses this mass sensitivity to control the deposition rate and final thickness of the material on the sample. When a voltage is applied across the crystal, it gets distorted and changes shape proportional to the applied voltage. At discrete frequencies of the applied voltage a condition of a very acute electro mechanical resonance is observed. When mass is added to the sensor facing

the gun, the frequency of these resonances is reduced. This change in frequency is repeatable and is presently precisely understood for specific oscillatory modes of the quartz. This phenomenon is the basis of measurement and process control tool that can detect the addition of less than an atomic layer of an adhered foreign material. Figure 3.3 shows a typical gold-coated quartz crystal.
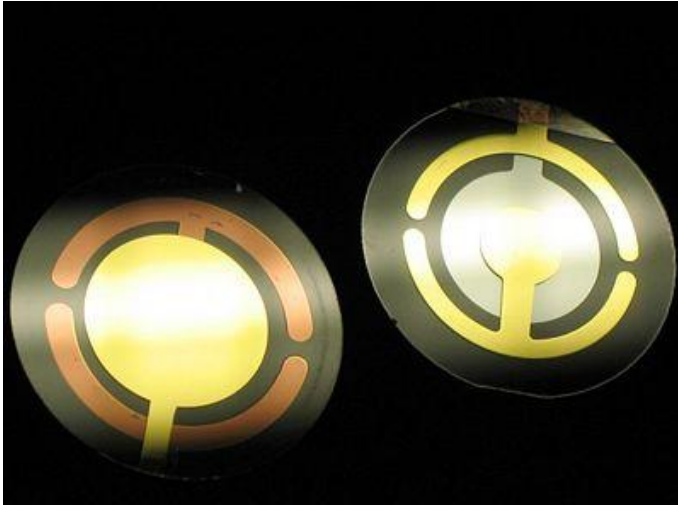


Fig. 3.3. Gold coated quartz crystal. [20]

For any deposition to happen in the desired way the pressure in the chamber should be of the desired value which is of utmost importance. As I have mentioned before we use two pumps (mechanical and turbo) and the use of an ion gauge to read the pressure. The gauge consists three electrodes which makes it function like a triode. The three electrodes for an ion gauge are the filament (cathode), collector or plate and a grid. When current is passed through the filament, electrons are emitted which have a forward and backward movement in front of the grid before finally entering it. In the process these electrons collide with gaseous molecules to form an ion-electron pair. This phenomenon is called electron ionization. The number of these ions is proportional to the

product of the gaseous ion molecular density and the current through the filament. These ions are collected in a plate or a collector to form an ion current. Since the gaseous molecule density is proportional to the density, by measuring the ion current we can estimate the pressure in the chamber.

The sources have individual shutter or shield as shown in the figures 3.1 and 3.2 which electro-mechanically operated to open and close whenever desired. The sample is held on graphite made sample holder, which is slid into rods to hold it in position in such a way that it has a direct path of visibility to the two elemental source guns. The substrate shutter operates same as the source shutter and is mainly operated during the start and end of the deposition. The heating filament over the substrate is used to heat the sample. The TEE, MP1 and MP2 valves shown in figures 3.1 and 3.2 are opened for the pumps to have access to pump the chamber.

## 3.2 Elemental Source Calibration

The quaternary Kesterite compound as we know has four elements associated to it namely copper, zinc, sin and selenium. Only when all these individual elements are deposited on to a film in the right quantities on to a substrate, we can actually form the compound irrespective of how ideal the process flow might be. The desired stoichiometry of a Kesterite compound should have Cu=25%, Zn= 12.5%, Sn=12.5% and Se=50%. So how do we know how much of each of these materials are depositing when we do the process. The deposition monitors operate on ideal conditions, which indicate how much of the material is depositing based on the amount of mass hitting the crystal sensor. To a certain extent we can relate this to the deposition of the same material on the substrate.

Though the flux hitting the crystal and the substrate could be the same, but we can never be sure that the amount of material sticking to the substrate is proportional to the flux reading of the deposition monitor. Sticking coefficient is one factor, which comes into play. Different materials have different sticking coefficient. It depends on various factors like roughness, type of material, etc. So how do we know exactly how much of the material hitting the substrate is actually depositing on it. The answer to it comes by calibrating each of the individual source elements.

Glass samples are taped and loaded into the chamber, we deposit the element to be calibrated for a certain time. Once the run is done we remove the tape from the sample and perform thickness measurement on it. Based on the thickness and taking the time into consideration. We actually get the rate of deposition of that element at a certain temperature in Angstroms per second. Like-wise multiple runs are done in the same fashion by increasing temperature at equal amount and a graph is plotted to show the rate of deposition at a certain temperature. This calibration of the gun gives an accurate measurement of the rate at which we are depositing each element. A model plot for the zinc source is shown in figure 3.4. The x-axis denotes the input voltage on the power controller and we can observe that there is a gradual increase in the rate as the temperature is increased.
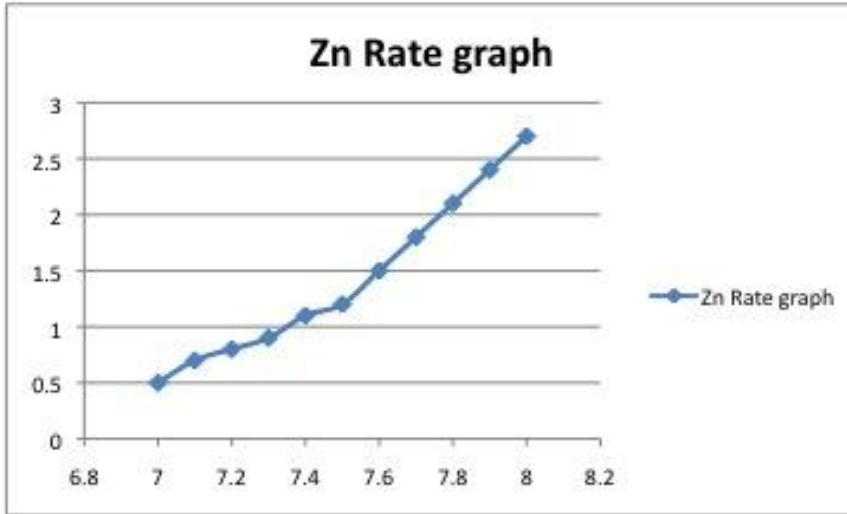
Fig. 3.4. Zn calibration plot. X-axis denotes the input voltage, y-axis shows the flux rate.

Thus by calibrating the individual elements we know the time for which each element is to be deposited to get the desired amount on the film to achieve stoichiometry. The problem of depositing one or more elements in excess would generate precursor compounds to form, which in turn would give more than one phase in the film. This is something as we know is not desired.

**3.3 Device Fabrication**

In this sub section I would list out all the fabrication procedures followed in making the Kesterite based solar cell. I personally deposited the CZSS layer(p type) and the CdS(n type) layers but all the sputtering based depositions (moly, i-ZnO, Al-ZnO) are done along with other research students in my group. A block diagram of the Kesterite-based solar cell is shown below in figure 3.5.
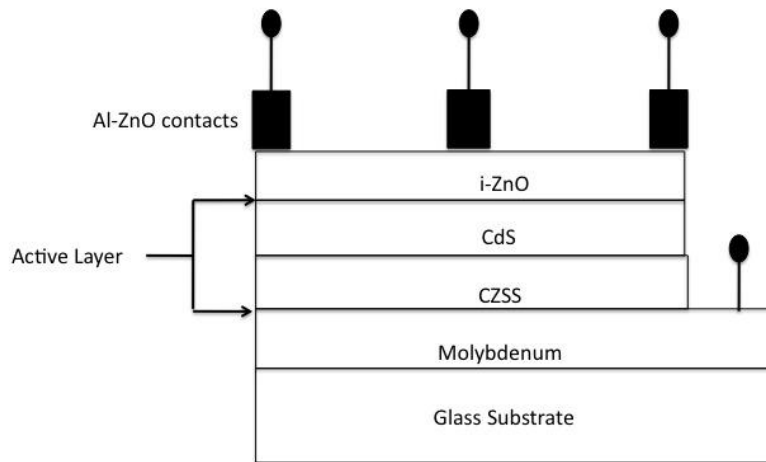
Fig. 3.5. CZSS based solar cell block diagram.

### 3.3.1 Substrate Cleaning

The glasses we used include soda lime and 7059 glass for material characterization and molybdenum coated soda lime glass for device fabrication. The soda lime glass substrate is first scrubbed with soap and rinsed properly in DI water. The samples are then dipped in methanol taken in a beaker and placed in the sonicator for 30 minutes. After this the sample is taken out and dipped in DI water and again put back in the sonicator for another 30 minutes. Once done the samples are blown dry using compressed nitrogen and ready to be loaded into the chamber.

The 7059 Corning glass is first rinsed in DI water to remove all the small particulates and gently scrubbed with a fine brush under DI water. Then the sample is dipped in a HF solution of 1:10 concentration with water for 10 seconds. The sample is

taken out and rinsed in DI water. This process is repeated once again and then blown dry with compressed nitrogen after which the sample is ready to go.

### 3.3.2 Moly Deposition

A bi-layer deposition of moly is done on cleaned soda lime glass using DC sputtering. The first layer done at a base pressure of 5 milli torr for a final thickness of 2000 angstroms is done for better adhesion to glass. Another layer on top of this for a thickness of 8000 angstroms is done at 3 milli torr for a smooth surface finish and high conductivity. The rate of deposition for both the depositions is maintained at 10 angstroms per second. Argon gas flow is used as a carrier. The moly acts as a back contact to the sample being tested for J-V measurements.

### 3.3.3 CZSS Formation

The moly coated soda lime glass is loaded into chamber 1 and Copper layer is deposited. The Sample is then loaded into chamber 2 and zinc is deposited over copper. We encountered problems in depositing zinc first because of its week sticking coefficient due to which it barely sticks to 7059 glass. After the Zn depositing the sample is taken out and loaded into chamber 1 again to deposit a sequence of runs in the order of Cu-Sn-Cu. Once this run is done we finally form a stack of 5 layers in the order Cu-Zn-Cu-Sn-Cu, where Zn and Sn are encapsulated between copper layers. The final step involves selenization of the sample under elemental Se flux at substrate temperatures varying between 300 to 500 degrees centigrade. The procedure would be well understood as we

discuss results in the next chapter by which we can understand the reason behind this process.

### 3.3.4 CdS Deposition

The CdS layer is deposited on the CZSS layer using ammonium hydroxide, cadmium acetate and thiourea. The process starts by preparing individual solutions of 74.5 ml of Ammonium hydroxide ($NH_4OH$), 59.6 ml of cadmium acetate [$Cd(CH_3CO_2)_2$], 59.6 ml of thiourea [$SC(NH_2)_2$] and 400 ml of DI water. First the ammonium hydroxide and cadmium acetate are poured into DI water in the amounts specified. The solution is then heated to 30 degrees centigrade. At this point thiourea is added to the solution and the temperature is heated to 80 degrees centigrade. Once it reaches 80 degrees the temperature is maintained for 7 minutes. At the end of the time the sample is taken out and rinsed under DI water for sometime to remove particulate matter on the sample and blown dry with compressed nitrogen.

### 3.3.5 I-ZnO Deposition

The intrinsic ZnO layer is deposited on CdS layer using RF sputtering. The material is deposited for a thickness of 1000 angstroms at a constant rate of 1 angstrom per second. Oxygen flow rate is controlled at 10% of the rate of argon.

### 3.3.6 Al-ZnO Deposition

The deposition of Al-ZnO is also done by RF sputtering under the influence of argon gas. A mask is laid on the sample to pin point the contact regions on the sample.

Desired thickness of 3000 angstroms is deposited at a rate of 1 angstrom per second. The Al-ZnO is used as top contact for the J-V measurements.

### 3.3.7 Device Isolation

Scratching off all the layers till we reach the moly layer along the grid pattern does the device isolation for each point of contact of the Al-ZnO. A back contact is made at an inactive region on the sample till the moly layer using a blade. Indium is used for better contact on the moly by melting it on moly for the back contact and avoids shorts with the Al-ZnO contacts.

### 3.4 Material Characterization

Below I would briefly describe all the methods used for material characterization. They would include Scanning electron microscope, and X-ray diffraction.

### 3.4.1 Scanning Electron Microscope

The scanning electron microscope is used on the samples made to study the lateral and cross sectional imaging. The SEM is mainly used on CZSS layers deposited on direct soda lime glass and 7059 corning glass to study the elemental composition in order to attain stoichiometry. A 200k X magnification is used to pin point the location on the sample we intended to study. Different ranges of operating voltages were used varying from 10kv to 25kv (max) based on the film thickness. As the electron beam reaches only into the first 5k angstroms into the sample we had to vary the thickness so as to get an accurate value for the composition of the films made.

### 3.4.2 X-Ray Diffraction

The X-ray diffraction is used on the samples to study the structural and phase information. A film area of 1 $cm^2$ is characterized along a range of $20 \leq 2\theta \geq 90$.

### 3.5 Device Characterization

The device characterization techniques I used include transmission, current voltage and external quantum measurements. They are discussed briefly below.

### 3.5.1 Transmission Measurement

All the samples prepared on 7059 glass are tested for their optical properties using transmission measurements. We use a Silicon crystal as reference to study the transmitted light through the sample. Light is passed through the sample and transmission is measured at different wavelengths varying from 400nm to 1100nm. The data obtained is used to study the bandgap of the material.

### 3.5.2 Current-Voltage (J-V) Measurement

All the devices are tested for their I-V measurements both under darkness and under light. The voltage is swept from -0.1-0.5 volts. And the corresponding current is plotted.

# 4. FILM GROWTH ANALYSIS AND RESULTS

## 4.1 Kinetics and Thermodynamics of Film Formation

By the end of chapter three we come to a point where we are ready to determine what exactly we have fabricated at each stage of different material depositions. It is very important to understand the optical properties and morphology of the CZSS layer in comparison with CIS and CIGS absorber layer to validate the potential of this material too make it to the large scale manufacturing level. This we can only do if we perform intense analysis and error correction of minute details and first determine its functionality at the cell stage.

From a manufacturing perspective it is advantageous to deposit metals and then selenized it with solid selenium source. Selenium is a highly volatile element in vapor phase and gets into every nook and corner of the chamber. Over that the content of selenium need to achieve desire stoichiometric films is high. This is a major concern and shortcoming in a vacuum based material deposition. This is not only costly but also produces rapid build up of Se content inside the reactors. At a manufacturing level this results in the need for frequent cleaning of the chambers and hence adds to downtime [21]. The main reason behind all this is because of the low sticking coefficient of Se to the growth surface. This in turn is because of two reasons, firstly because of the formation of chains and rings by Se [21] and secondly due to the kinetics and

thermodynamics of surface interactions. The figure below shows a plot as to how much the ratio of Se with metal flux ratios is dependent on the operating substrate temperature [21]. It clearly shows that by operating at a higher substrate temperature of the film at 500 degrees we almost achieve the desired amount of Se content (50%) in the film as compared to 300 degrees for the same flux rate. This observation was done on CIGS films and might not behave the same with respect to Kesterite material.
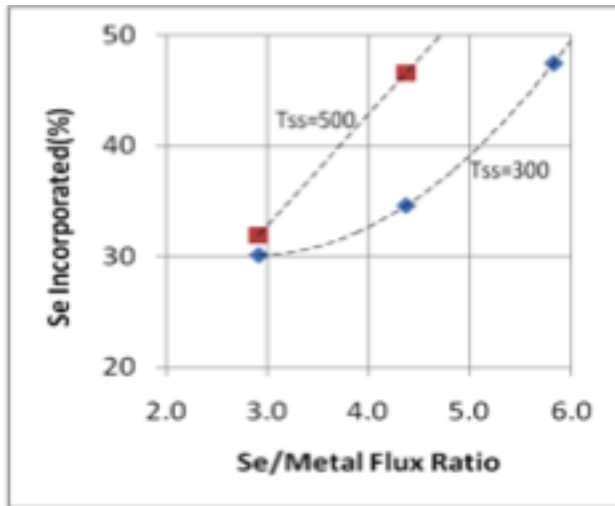


Fig. 4.1. Se incorporated in a CIGS film. [21]

Compound formation from Selenization of metal precursors is a complex of kinetics and thermodynamics. Kinetics deals with the diffusion of metals through other metals and compounds. And thermodynamics is the formation of compounds from precursors, which can be metals or precursors binaries of MSe with temperature as the variable. As I have mentioned before we form the stack of metals in the order Cu-Zn-Cu-Sn-Cu, based on which most of the copper is present at the moly interface and zinc and tin on top of it sequentially. The objective of forming CZSS is greatly dependent on

getting all these metals to reach a common place where they see Se flux at the desired amount to form the Kesterite compound at an optimum temperature.

The access of Se to the metals and how it actually forms binaries of MSe is not really known. But we can postulate two scenarios, which could be occurring. (1) All the metals diffuse to the surface region and when present in individual desired quantities and the optimum thermodynamic temperature see Se and form CZSS. (2) The Se itself diffuses through the metals reaching the surface and also their binaries with Se to reach metals buried underneath to form precursors with those metals or CZSS itself. To understand this we need to have a clear picture of the diffusion scenario of how each metal diffuses. Thus we conducted an experiment where we deposited metals with their operating temperatures and duration in the following way Cu (1185° C) for 50 min, Zn (295° C) for 95 min, Cu(1185°C) for 5 min, Sn (1200°C) for 50 min and finally Cu (1185°C) for 5 min. Once we formed this stack we selenized it at Se (205°C) for 95 min at a substrate temperature of 300°C to form a film. The sample is then tested for its composition using Energy dispersive spectroscopy (EDS) using a scanning electron microscope. The sample is annealed multiple times and similar testing is performed on it, the reason for this would be explained as we go along in the discussion.

Table 4.1. EDS results of CZSS 50 sample after each anneal.

| Source temperature & Time | | | | Sub. Temp | At%(EDS) | | | |
|---|---|---|---|---|---|---|---|---|
| Cu | Zn | Sn | Se | | Cu | Zn | Sn | Se |
| 1185 | 295 | 1200 | 205 | 300 | 14.08 | 29.23 | 29.64 | 27.06 |
| 50+5+5 | 95 | 50 | 95 | | | | | |
| | | | 205 | 300 | 13.38 | 30.57 | 24.92 | 31.14 |
| | | | 95 | | | | | |
| | | | 205 | 400 | 36.1 | 14.64 | 3.52 | 45.75 |
| | | | 95 | | | | | |
| | | | 205 | 400 | 34.61 | 9.14 | 6.77 | 49.49 |
| | | | 95 | | | | | |
| | | | 205 | 400 | 33.47 | 6.98 | 9.21 | 50.35 |
| | | | 95 | | | | | |
| | | | 205 | 400 | 33.2 | 9.22 | 8.31 | 49.28 |
| | | | 95 | | | | | |

After the first anneal at 300°C we see that we are CU poor (14.08 % which is supposed to be around 25%), Zn and Sn are very high than needed at around 29% each and Se at 27% which almost half of what we desire. This explains the diffusion of metals at 300°C in the following way. Cu which is the lower most layer in the stack, started to diffuse up to the surface passing through Zn and Sn. The Zn also diffused through Sn to the surface and the Sn, which is already predominantly present at the top of the stack, remained there. The Se content at 27% indicates that the metals are still not selenized properly, which also confirms the presence of various metal and MSe binary precursors to be present in the film.

So we anneal the sample again maintaining both the substrate temperature (300°C) and Se flux as the same as the first selenization run. The EDS shows numbers similar to the first anneal. Thus we can understand two phenomena to be occurring at this situation. (1) Operating the substrate temperature at 300°C isn't doing justice for our objective to bring all elements to the surface to form CZSS. Thus we need to vary the substrate temperature to understand and improve the diffusion phenomena of each individual metal. (2) As we have discussed before the sticking coefficient of Se depends on the operating substrate temperature. Thus operating the temperature at 300°C isn't getting enough Se to react to the growth surface as we desire. Based on our above two conclusions we decided to increase the substrate temperature to 400°C in the next anneal step. The EDS after the third selenization run gave us results, which were different from the previous results. Before we discuss the results we should always keep in mind that the EDS can just see the top 1-micron of the estimated 5-micron thick sample. What ever is present below that is not known by EDS testing on the sample. So coming back to EDS

results after the third selenization run the Cu shot up to 36% from 13% which shows that Cu diffuses very easily through both the other metals and reached the surface where it could now see Se. The Zn and Sn dropped down to 9% and 6% from 30% and 24% respectively. And Se reached 46%, which is pretty close to what we want. Thus we can now understand that Cu diffuses better than Zn and Sn to the surface. The Zn and Sn are buried under the Cu and thus their right amounts in the sample cannot be determined using EDS as it can only see the top 1-micron of the film. After which additional anneals were performed on the same sample to see if the Zn and Sn would come up to the surface, but the EDS results didn't show much change. The figure 4.2 shows the composition for each of the constituents after each anneal step based on the EDS data. The plots for each of the metals show how they move along after each anneal step in the top 1-micron of the film. Thus we can summarize the above in the following few sentences. Initially all the metals are around the same Atomic percentage after the first and second anneal at 300°C. At 400°C Cu diffuses rapidly to the surface and is selenized. Sn is pushed back by Cu diffusing through it while some Zn remains in the EDS area. With further anneal steps Zn approaches its deposited value indicating it has spread uniformly. Sn climbs back up to attain the same composition as Zn(10%) indicating perhaps the formation of CZSS. Thus we can expect the top 500 nm to contain CZSS and CuSe due to large Cu presence.
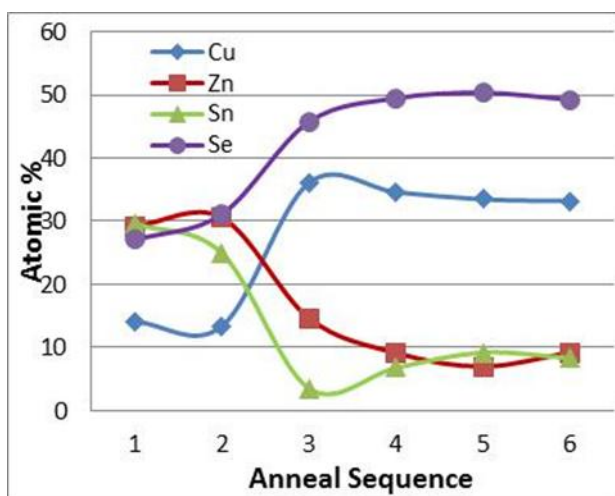
Fig. 4.2. Film composition as a function of number of anneal times.

After the first anneal step in the sample CZSS 50 we know we don't have enough Se content in the film. Though we expect some part of the film to be Kesterite material, the remaining film could be occupied by other phases present due to the insufficient Se content and also the operating substrate temperature. Based on the background knowledge of this film we know a large portion of these secondary precursors would have ZnSe, $Cu_2SnSe3$ and binaries of CuSe. These intermediate phases as well as the desired CZSS form according to phase diagrams and forming energies. The phase formation can occur at the top surface of the film and also in the bulk of the film. Since Cu diffuses well to the top surface we can expect binaries of copper selenide to be present at the surface. From Ahns paper we know that the ZnSe is generally found at the moly/CZSS interface and $Cu_2SnSe_3$ would be present in the bulk of the film, as we know Sn does not easily diffuse to the surface even after repeatedly annealing the sample. Thus

59

the initial few runs were done to understand the kinetics of the individual metal and MSe binary precursors in the film.

We have tried various orders of deposition of metals before they are selenized. The table below shows the different ways we implemented to synthesize the CZSS material and the problems we faced in doing so.

Table 4.2. Different order of depositions implemented.

| Glass Type | Procedure | Observation |
| --- | --- | --- |
| 7059 | Zn/Sn-Cu-Selenization (300°-500°) | Loss of Zinc |
| 7059 | ZnSe-Sn-Cu-Selenization (300°-500°) | Flaking , Non Uniform, ZnSe not reacting |
| 7059 | Cu/Sn-ZnSe-Selenization (300°-500°) | Flaking |
| 7059 | Cu/Sn-Zn/Se (300°-500°) | Flaking, Loss of Zinc |
| 7059 | Zn/Se-Cu/Sn-Selenization (300°-500°) | Puffy look, non-uniform |
| $SnO_2$ | Zn/Se(275°C)-Cu/Sn-Selenization (300°-500°) | ZnSe at the glass, Flaking |
| $SnO_2$ | Zn-Cu/Sn-Selenization (300°-500°) | Non-uniform Zn in step 1 |
| $SnO_2$ | Cu-Zn-Cu-Sn-Cu-Selenization (300°-500°) | EDS picking up Sn from the glass |

Table 4.2. (Continued)

| 7059 | Cu-Zn-Cu-Sn-Cu-<br><br>Selenization (300°-500°) | Good uniform samples |
|---|---|---|

Looking at the table above, we observed the problems, which we encountered by depositing the metals in different ways. Thus we came down to stacking the metals and then selenizing it, which gave us uniform samples with no flaking problem.

Our primary tool of determining the composition of the films formed is Electron Dispersive Spectroscopy (EDS) using a Scanning Electron Microscope. But the disadvantage of this technique is it only sees the top 500nm of the film. Thus what material is present underneath it is not studied. The diffusion phenomenon of each metal observed in the figure 4.2 would be the same even if we made a thinner film. In order to determine the right composition of a film we need to resort to making thinner films by which the EDS could scan through the entire thickness of the film.

There is evidence that heating a film containing Zn above 300°C in the absence of Se flux can cause the Zinc to diffuse to the surface and leave the film. This peculiar phenomenon is not the same with respect to Cu and Sn. The anneal procedure we followed till now during Selenization process was that we made the film see Se flux only after the substrate temperature reached its set value ranging from (300°-500°C). But those films where the substrate temperature is higher than 300°C, the EDS results indicated barely any zinc left in the sample. These were observed on thinner films in order to avoid the conflict of the limitations of EDS. The table below indicates the EDS results.

Table 4.3. Controlling loss of zinc

| Cu | Zn | Sn | Se | Sub. Temp. | Cu(At%) | Zn(At%) | Sn(At%) | Se(At%) |
|---|---|---|---|---|---|---|---|---|
| 1185(Temp.) 10+1+1(min) | 295(Temp.) 13(min) | 1200(Temp.) 4(min) | 210(Temp.) 30(min) | 350 | 23.22 | 3.12 | 19.63 | 54.03 |
| 1185 10+1+1 | 295 13(Blue) | 1200 4 | 210 30 | 400 | 27.69 | 3.09 | 17.47 | 51.75 |
| 1185 10+1+1 | 295 13(Blue) | 1200 4 | 215 40 | 300+400 | 14.75 | 18.28 | 12.53 | 54.44 |
| 1185 10+1+1 | 295 13(Blue) | 1200 4 | 215 40 | 300+350 | 11.43 | 26.34 | 7.84 | 54.4 |

The table indicates the first two runs where the sample is heated to its set substrate temperature after which it starts to see selenium flux. We can see that the Zinc percentage is very low though and we are sure we have enough Zn present in the metal stack we formed before Selenization. Thus we came to the conclusion that the Zn leaves the film when heated above 300°C with no Se flux. In order to counteract this problem we came up with a new anneal procedure by which we completely controlled the loss of Zinc. This procedure involved a two-stage process. We heated up the sample to 300°C where we selenized it for 20 minutes as we know we do not lose Zn at this temperature. This step helps the metals to properly diffuse within each other as we have explained earlier in the diffusion phenomenon. In the second step we increased the substrate temperature to 350C or 400°C based on the experiment where we again selenized the sample for 20 minutes. Another modification was that we made the sample see Se flux once it reached 200°C while heating up to 300°C and while cooling down till 250°C at the end of Selenization. The results were very much distinguishable to the films done in the old method.  As we can see in the table above we actually have more zinc than required, which we completely lost in the old anneal method. Thus now we had to reduce the amount of zinc content to attain perfect stoichiometric films.
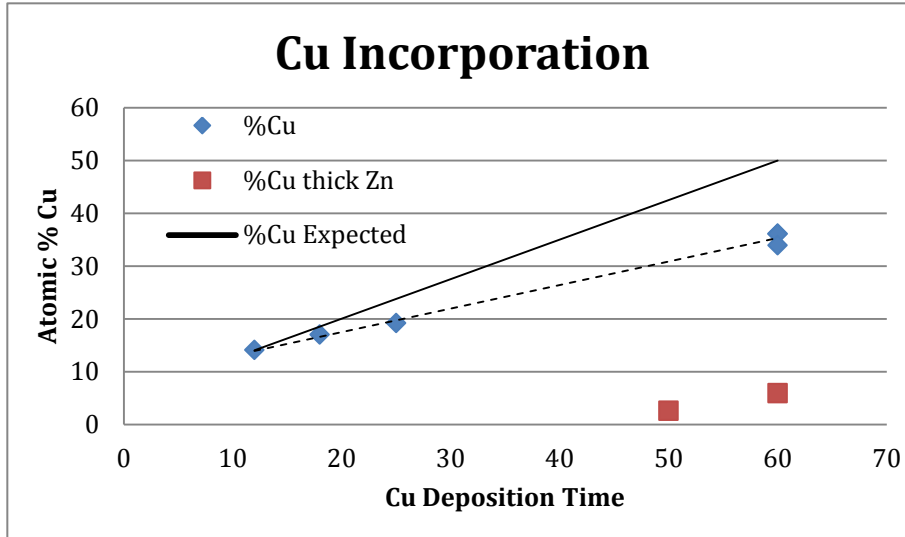
Fig. 4.3. %Cu variation under the new anneal procedure when we retain Zn.

Previously when we were using the old anneal procedure, the %Cu observed in the EDS is proportional to the Cu deposition time. The reason behind this as we know Cu reaches the top surface faster than any other precursor metal and gets selenized. But we also know we lost Zn in the film. But after we started using the new anneal procedure, we observed that the %Cu read by the EDS is less than what is expected. Thus is prevented to reach the surface as used to by the Zn. This is shown in the figure 2.4.

## 4.2 XRD Analysis

Now that we have made films which are close to the stoichiometry we desire, we proceed forward in analyzing it with XRD through which we hope to determine what phases we form. We swept the sample through a range of $20° \leq 2\theta \leq 80°$ where we observed peaks which correlate to the CZSS material. The plots below shows the XRD analysis and its corresponding stick pattern for the CZSS 50 sample.
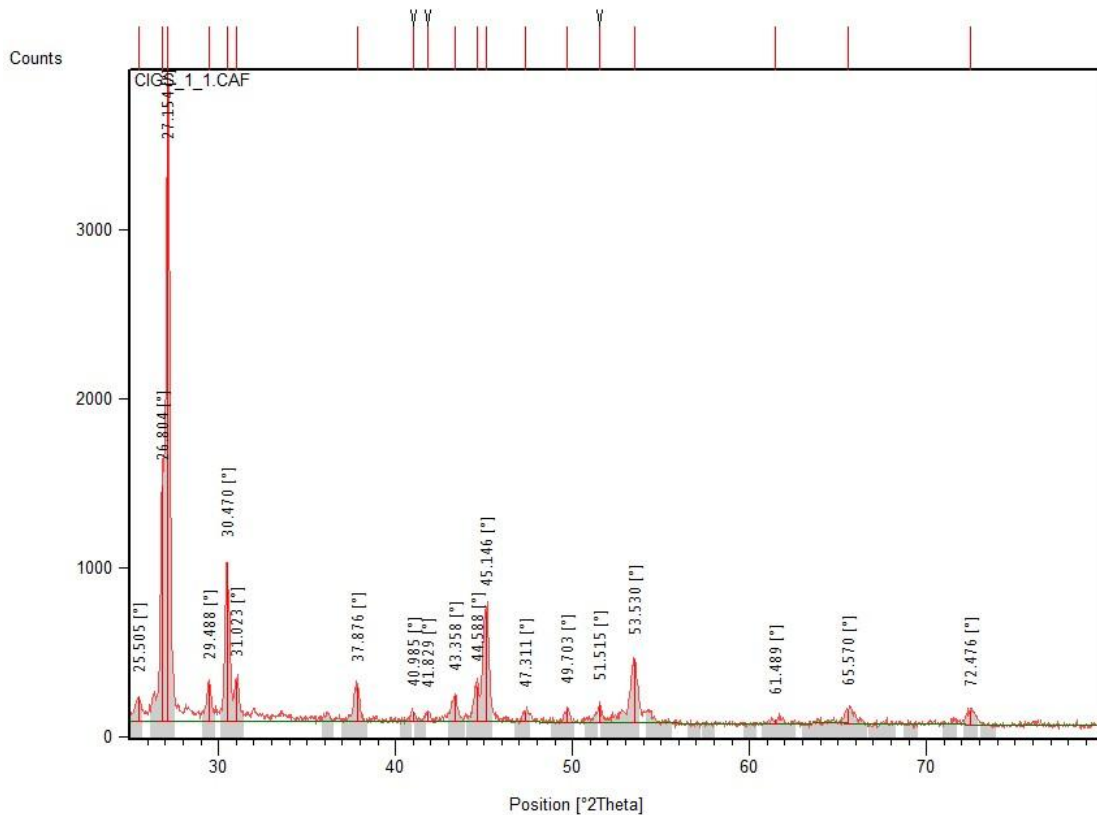
Fig. 4.4. XRD for CZSS 50.

The plot above shows strong peaks at angles of 27.154 and 45.146 which correspond to the CZSS material. We know from our background knowledge that ZnSe peaks perfectly coincides with the CZSS peaks. Another important observation we made was that Copper Tin Selenide, which is one other possible phase formation also coincides with the CZSS and ZnSe peaks, which makes it even more complicated. Thus we have to distinguish between the peaks of these three materials to determine what material we are forming, which is to some extent a limitation on XRD.

In XRD, the beam is scanned along the sample over a certain length, but because we are dealing with very thin films here of the order of 1 micron this technique is

questionable to be accurate. Thus an advanced technique in XRD called the grazing incidence is used on our samples where the sample holder is not rotated and the beam hits the sample at minimal angle at around 0.5-1° with respect to the surface. Thus the beam grazes along the surface because of which the beam sees more of the sample now though it's a very thin film. This technique was used on all the samples we have done and we could observe better-defined peaks as compared to the old procedure.

In order to carefully compare and differentiate the XRD plots of all the three materials (CZSS, ZnSe and $Cu_2SnSe_3$), we have made our own ZnSe and $Cu_2SnSe_3$ samples. Plots for CZSS 84 & 88 done at substrate temperature 350°C and CZSS 85 done at substrate temperature 400°C are shown below sequentially.
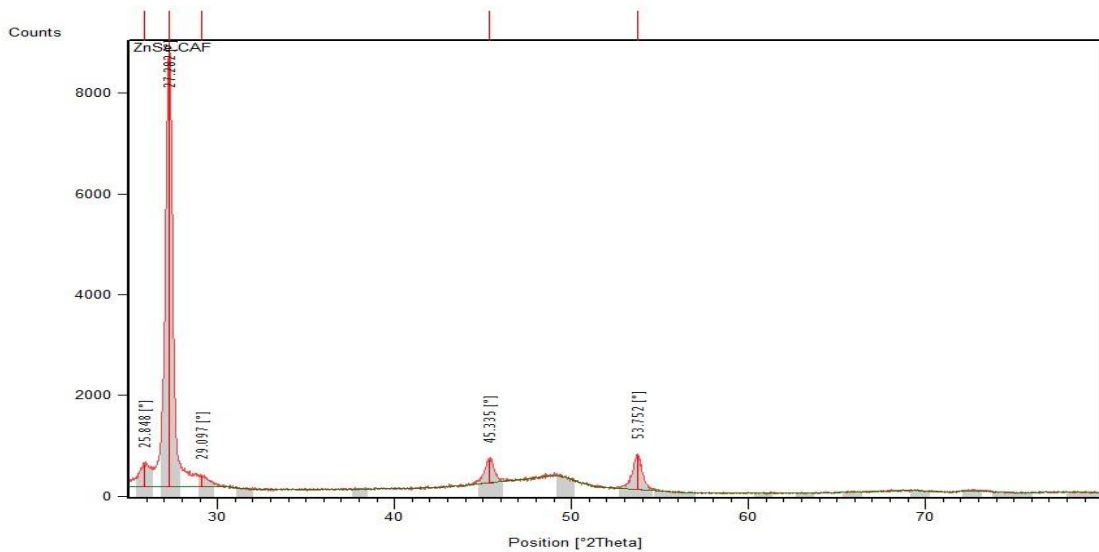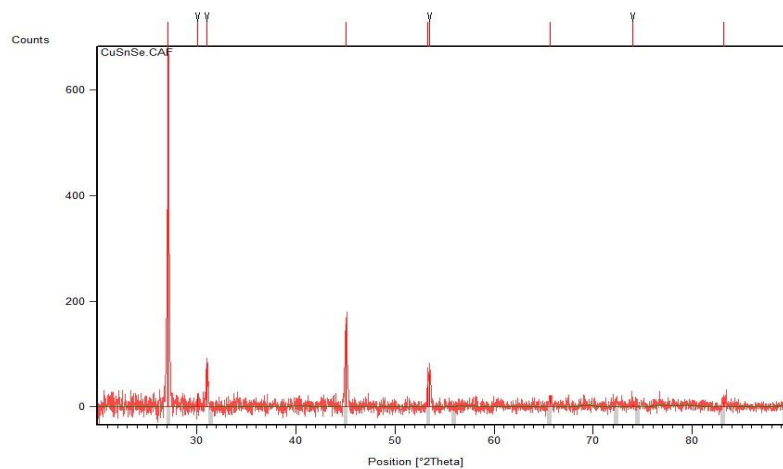


Fig. 4.5. XRD plot for ZnSe.
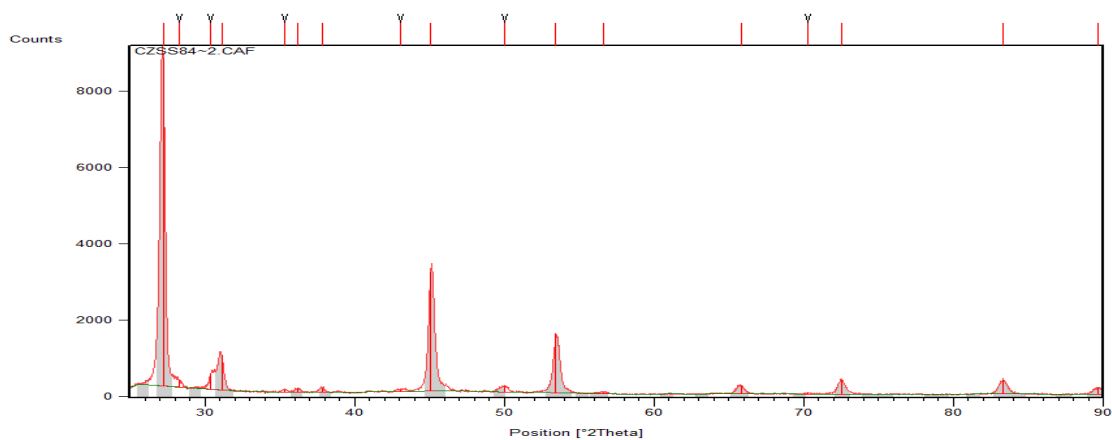
Fig. 4.6. XRD plot for $Cu_2SnSe_3$.



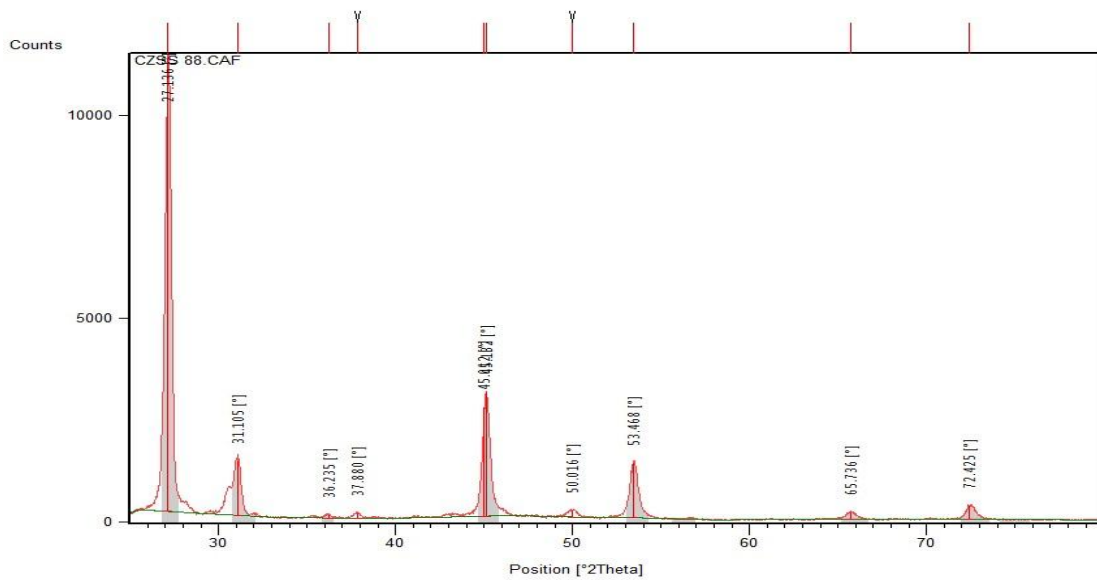Fig. 4.7. XRD plot for CZSS 84 done at 350°C.
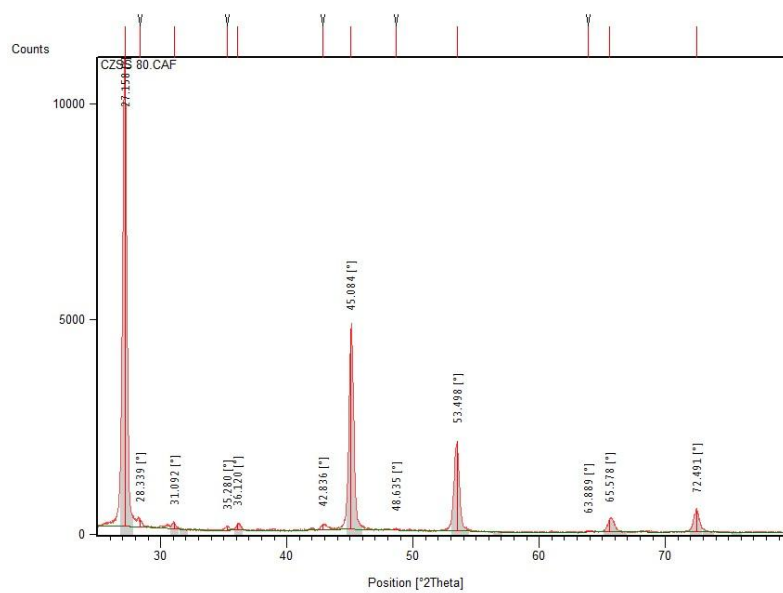
Fig. 4.8. XRD plot for CZSS 88 done at 350°C.



Fig. 4.9. XRD plot for CZSS 85 done at 400°C.

If we observe the above plots, we can come to a conclusion that irrespective of the material (CZSS, ZnSe and $Cu_2SnSe_3$), the XRD peaks are positioned the same based on their 2θ angles. But if we closely observe the ZnSe plot, there are two peaks at angles 25° and 29° which are not present in either the CZSS or the $Cu_2SnSe_3$. If we look at the plot for CZSS 50 we see these peaks present in them too. But we need to remind ourselves of the fact that CZSS 50 is not a stoichiometric film. Thus we can conclude that if our CZSS films do really have ZnSe, then we should be able to see these two peaks. Another important conclusion we need to make here is, because we know that our films CZSS 84,85 & 88 (irrespective of the substrate temperature) are stoichiometric films based on the EDS data, and if we do not have ZnSe in them then we should not have $Cu_2SnSe_3$ as well.

The stick pattern of CZSS 88 is shown below in fig. 4.10. The peaks of CZSS and copper tin selenide perfectly coincide with the peak list but we can observe a minor variation with respect to the ZnSe peak. Also there few peaks in the peak list which can be only observed in the CZSS peaks. The Ahns paper indicates that there is no such variation in their XRD analysis done at different substrate temperature as indicated in chapter 2, but they do not consider the possibility of Copper Tin Selenide at all. This could be due to that fact that they report the loss of Sn in their films went operating at higher temperatures, which is not the case with our films. Irrespective of the temperature we performed Selenization at, we could observe the presence of Tin at its desired level.
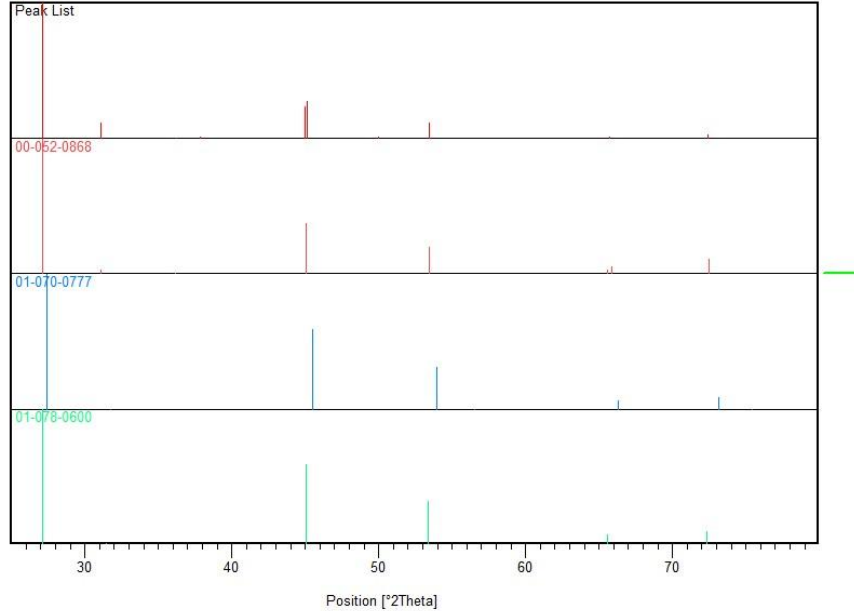
Fig. 4.10. Stick pattern for CZSS 88, peak list indicates the observed peaks, Red- CZSS, Blue- ZnSe and Green- $Cu_2SnSe_3$.

Based on the XRD plots it is most likely that the film is CZSS and not ZnSe or $Cu_2SnSe_3$. But we cannot completely ignore the presence of both these materials in our films. Maybe they are present but in trace amounts. Thus we can conclude saying that the XRD data is definitely supportive but not conclusive.

## 4.3 Bandgap Determination

All the samples we have made are studied optically by doing transmission measurements on them. The observed data was used to plot the absorption coefficient of that sample to compare with the information we have from the Ahns paper and standard CIS plot.

70

The Standard band gap value of CIS is said to be around 1eV, which is where we expect the CZSS bandgap to be, as no concrete data is available stating its bandgap value. Ahns paper indicates his bandgap values of sample done at 320°C and 400°C with blue and brown lines respectively as shown in the figure below. He says the shift in bandgap is because of the presence of ZnSe at higher temperatures. Our samples done at 400 Degrees coincide perfectly with those of Ahns plot at 400 degrees.
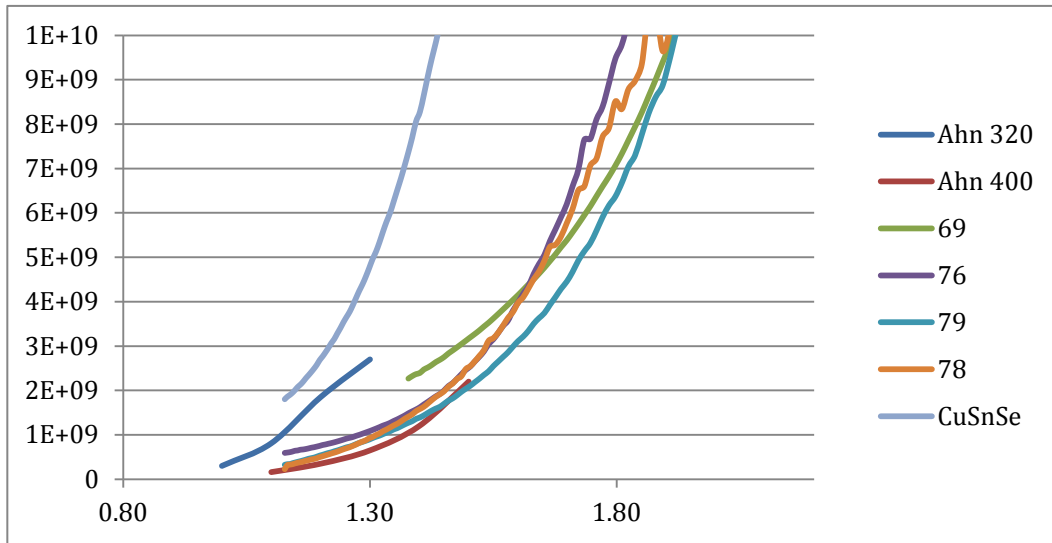


Fig. 4.11. Our bandgap plots in comparison with Ahns and copper tin selenide.

In this figure 4.6 we give a comparison of our samples done at 400 degrees in comparison with Ahns plots at 320°C and 400°C degrees and the copper tin selenide plot. Ahn reports that his sample done at 320° is CZSS material. He feels that XRD is not an accurate method of determining the material we are forming, thus resorting to bandgap plots to determine the material being formed. All our plots of samples done at 400°C coincide with Ahns 400°C plot, indicating some ZnSe presence. Thus we need to observe if it's the same case when we make our samples at 350°C as well. The plot of copper tin

selenide distinguishes itself from all other plots based on bandgap as indicated in the figure 4.11.
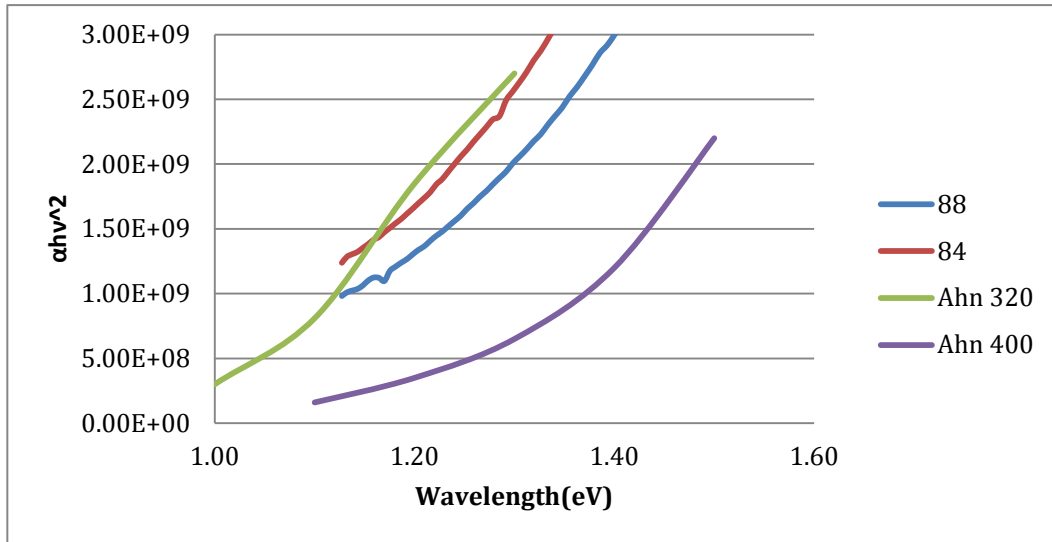


Fig. 4.12. CZSS films done at 350°C in comparison with Ahns plots.

Samples 84 and 88 were selenized at 350°C and their optical properties are measured and compared with Ahns samples done at 350°C and 400°C. CZSS 84 sample is Zinc poor with metal ratios of Zn/Sn = 0.77 and Cu/(Zn+Sn) = 1 as compared to CZSS 88 whose ratios are Zn/Sn = 1.39 and Cu/(Zn+Sn) = 0.67. Both the plots of these two samples are close to the Ahns sample done at 320°C but the CZSS 84 almost coincides with it. Thus the Zinc percentage in the sample affects its position in the bandgap plot though both are operated at the same substrate temperature. However, it is apparent that substrate temperature is the dominant variable.
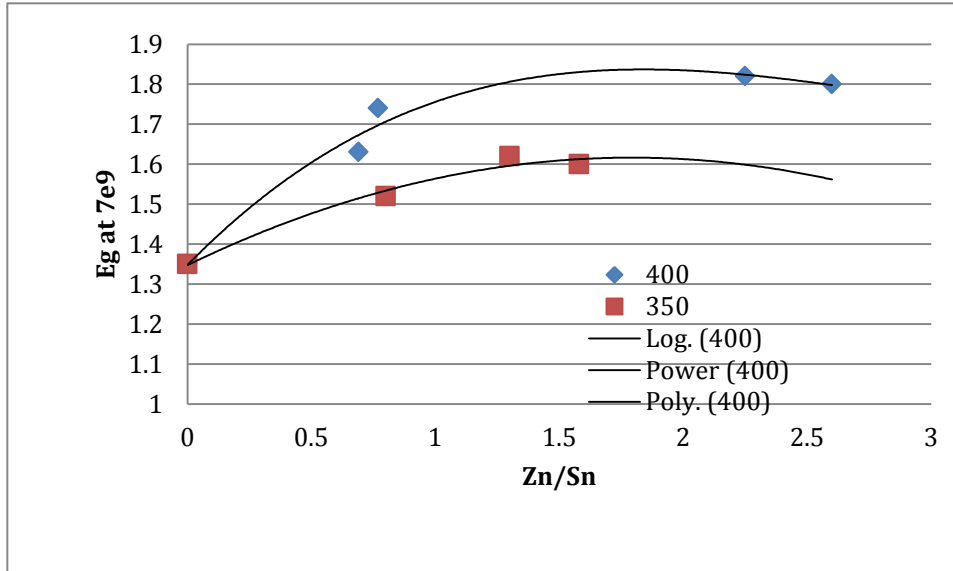
Fig. 4.13. $(\alpha h\nu)^2$ vs Zn/Sn ratio of films done at 350°C and 400°C.

The above plot shows the $(\alpha h\nu)^2$ vs Zn/Sn ratio of films done at 350°C and 400°C. If the Zn/Sn ratio is increasing, ideally the plot should be linear till 2.5, which corresponds to the bandgap of ZnSe. But we observe that the plots are saturating and not linearly increasing as we increase Zn/Sn ratio.
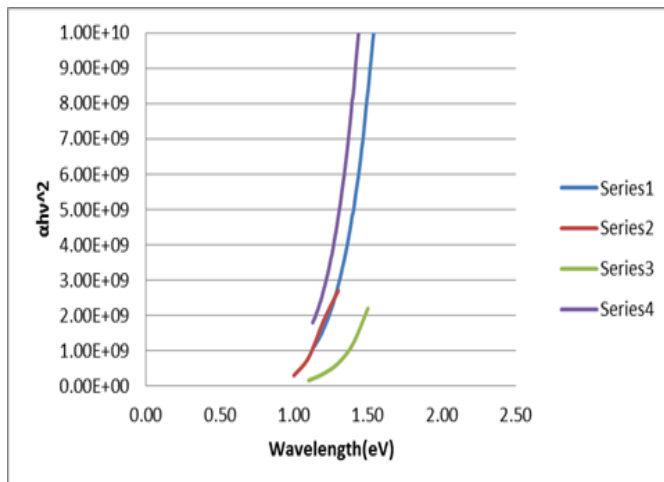


Fig. 4.14. Series 1: Film with only ZnSe & $Cu_2SnSe_3$, Series 2: Ahn 320°C, Series 3: Ahn 400°C and Series 4: $Cu_2SnSe_3$.

So what if all the Zn was forming ZnSe and Cu and Sn were forming $Cu_2SnSe_3$? In order to know where the plot for bandgap for such a sample would be we determined the position for such a sample by adding the approximate thickness of Zn in a $Cu_2SnSe_3$ film sample we have done. The plot as we can see in the figure 4.14 perfectly coincides with the Ahn 320°C plot. Thus this begs the question about the phase composition of all our films done at 400°C. What is the phase composition of all these films, which makes their bandgap to shift to higher bandgap values than 1 eV. We are not sure at the moment about the phase composition of the films at 400°C. Thus we can conclude saying that our films at 350°C do have most of CZSS based on the Ahns 320°C plot and also on the XRD results but for films done at 400°C we are not really sure of the phase composition though we know we don't have much of ZnSe in them based on XRD results.

## 4.4 Device Results

Now that we studied the film's optical properties and XRD, we now try to encapsulate the CZSS film between molybdenum and CdS layer, with ZnO layers on top to make fully functional devices. At this point of time we could not make many samples to study the device characterization. All the dots are tested both in darkness and under light. The voltage is swept and the corresponding current is noted.

Most of the dots are acting as resistors and there is no convincing data we could present at the moment. The I-V plots for a dot which we felt had some life in it is shown below. There are few aspects we still need to work on to improve the device characterization results. Firstly the non-uniformity of CZSS on moly samples. Secondly to control the particulate formation during CdS layer deposition. Thirdly both the ZnO

74

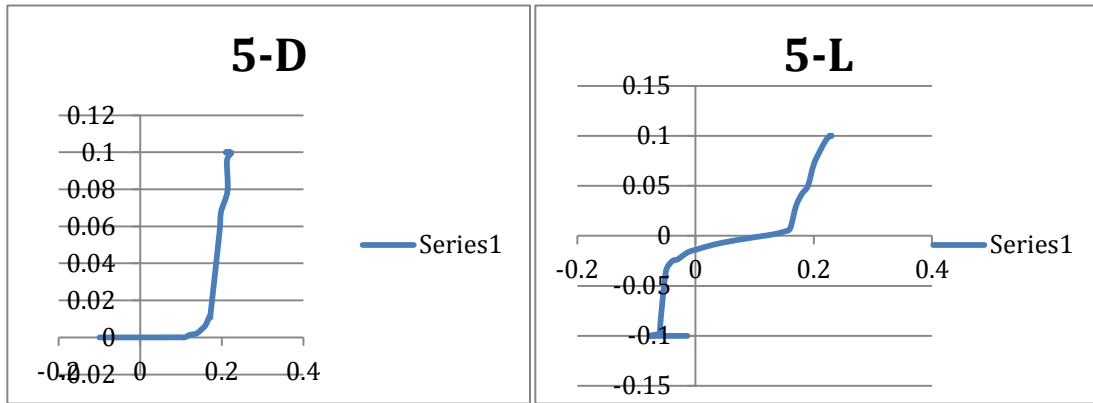and Al-ZnO layer, where we are trying to optimize the substrate temperature and thickness.



Fig. 4.15. Left: I-V in darkness, Right: I-V under light.

# 5. CONCLUSION

Our objective of this study was to synthesize the Kesterite material in a process flow, which is advantageous at a manufacturable stage with no secondary phase formation. We have understood the way by which the metals move through each other during selenization achieving the desired ratio of Zn/Sn to be 1. Thus the potential kinetic and thermodynamic barriers to forming films this way seem not to be insurmountable. Using the new anneal procedure which could counteract many problems we faced before like losing zinc. The Films were made at stoichiometric metal ratios at different substrate temperature varying from 300-500°C. Our XRD plots indicate supportive results that we are forming the Kesterite material though not conclusive. Based on the optical measurements we could conclude that we are forming the Kesterite material in comparison with the Ahns paper. However we wish to fine tune our understanding on the optical properties of this material at films done at temperature higher than 350°C. As a future work we also have to modify the i-ZnO, Al-ZnO depositions to increase conductivity and performance of the final device. But the advantage we hold is the process flow, which is easier to go through at a manufacturable level.

# REFERENCES

1. http://en.wikipedia.org/wiki/Population

2. http://en.wikipedia.org/wiki/Renewable_energy

3. http://www.resourceinvestor.com/News/2009/2/Pages/Hot-Rocks-Equals-Hot-Stocks-.aspx

4. http://www.greentechhistory.com/2009/03/renewable-energy-cost-curves-1980-2020/

5. J.C. Bernede, LAMP, FSTN, Université de Nantes, 2 Rué de la Houssinière, BP 92208, Nantes CEDEX 3, 44322, France.

6. http://www.physicsforums.com/library.php?do=view_item&itemid=30

7. http://en.wikipedia.org/wiki/Photovoltaics

8. http://www.energy-green.net/blog/articles/solar-energy/PolycrystallineThinFilmSolarCellSolarEnergyTechnology.html

9. http://pvcdrom.pveducation.org/DESIGN/NORFLCTN.HTM

10. http://www.busytrade.com/selling-leads/545707/Silicon-Ingot.html

11. http://en.wikipedia.org/wiki/Solar_cell

12. http://www.science.org.au/nova/newscientist/027ns_005.htm

13. G. Zoppi, I. Forbes, R. Miles, P. Dale, J. Scragg and L. peter, Prog. Photovolt. Res. Appl. 17:315(2009).

14. S. Ahn, S. Jung, J. Gwak, A. Cho, K. Shin, K. Yoon, D. Park, H. Cheong and J. Ho Yun, Appl. Phys. Lett., 97,21905(2010).

15. O. Volobujeva, E. Mellikov, J. Raudoja, M. Grossberg, S. Bereznev, M. Altosaar, R.Traksmaa.2008IEEE.

16. Philip J. Dale, Katja Hoenes, Jonathan Scragg, Susanne Siebentritt; 2009 IEEE.

17. Katagiri, H., et al., *Applied Physics Express*, 2008. 1(4).

18. Siemer, K., et al., *Sol. Energy Mater. Sol. Cells*, 2001. 67(1-4): p. 159-166.

19. AbuShama, J.A.M., et al., *Prog. Photovoltaics*, 2004. 12(1): p. 39-45.

20. http://en.wikipedia.org/wiki/Quartz_crystal_microbalance

21. K. Jayadevan, R. Anders, S. Zafar, C. S. Ferekides, D. L. Morel; Hawaii 2010 IEEE.

22. http://www.webelements.com/compounds/zinc/zinc_selenide.html

23. http://bentgroup.stanford.edu/Research/research_PVmaterials.html